A Model-Based Receiver for CPM Signals in a Cochannel Interference Limited Environment

by

Pierre Barthelemy

Thesis submitted to the Faculty of the
Virginia Polytechnic Institute and State University
in partial fulfillment of the requirements for the degree of

Master of Science
in
Electrical Engineering

Brian D. Woerner, Chair

Amy E. Bell

Jeffrey H. Reed

May 2002

Blacksburg, Virginia

Keywords: Parametric Frequency Estimation, Cochannel Interference, MSK, Equalization

A Model-Based Receiver for CPM Signals in a Cochannel Interference Limited Environment

by
Pierre Barthelemy
Committee Chairman: Brian D. Woerner
Electrical Engineering

Abstract

Cochannel interference (CCI) is a major impairment in narrowband cellular systems. To increase the spectral efficiency of the narrowband systems, identical carrier frequencies are reused in distant cells. The interference rejection capability of the receiver determines this frequency reuse and is therefore critical. In this thesis, we propose an improved demodulation scheme, employing high-resolution frequency estimation techniques, for continuous phase modulated (CPM) signals in presence of CCI. Minimum shift keying (MSK), which is a special case of CPM, is a very popular modulation format around the world. Frequency detectors, such as the limiter-discriminator permit the non-coherent demodulation of MSK signals. High-resolution frequency estimation appears as a very attractive alternative to the conventional non-coherent frequency detectors. The frequency estimation methods that we have studied are based on autoregressive modeling.

The contributions of this thesis include the implementation of various demodulation schemes employing parametric frequency estimation. The use of the Viterbi algorithm as a non-linear equalization technique to mitigate intersymbol interference is considered. We verified that the model-based sequence estimation schemes outperform the conventional non-coherent receivers for MSK with AWGN, flat fading, and CCI. Demodulator diversity is also investigated as a way to combat interference. An improved technique combining the proposed model-based receiver and the conventional coherent receiver is implemented and simulated in presence of CCI.

Acknowledgments

Foremost I would like to thank my advisor, Dr. Brian D. Woerner, for his support and guidance. I am sincerely grateful to him for giving me the opportunity to work at the Mobile and Portable Radio Research Group (MPRG) among excellent students and with a very cooperative staff. I wish to express my gratitude to my committee members, Dr. Amy E. Bell and Dr. Jeffrey H. Reed, for their encouragements and for reviewing this thesis.

During the course of this thesis, it has been a pleasure to work with Yasir Ahmed on frequency estimation. I also thank all of my friends from MPRG for their help on technical and non-technical matters.

This research has been sponsored by the MPRG Industrial Affiliates program, the Defense Advanced Research Project Agency (DARPA) and Raytheon through the ACN project.

Contents

List of Figures

Chapter 1 Introduction

Time division and frequency division multiple accesses are two techniques employed in typical narrowband systems to separate the users from identical cells. For adjacent cells, the users are separated by employing distinct carrier frequencies. These carrier frequencies are reused in distant cells such that the propagation loss attenuates the interference between the cochannel users. However to cope with the rising number of users, the cell size and the frequency reuse factor are reduced, resulting in an increase in the level of cochannel interference (CCI). In consequence CCI has become the major limitation to the capacity of cellular systems.

The use of antenna arrays has opened the door to a new dimension of cellular systems: spatial division multiple access. Sectorization permits a great reduction of cochannel interference and a large increase in the capacity of current systems. However, antenna arrays can be used only to a certain extent; cost, power, and complexity are some of the factors that restrain the number of antenna elements employed. As a result, base stations equipped with antenna arrays may still experience interference from a few co-channel users. In the specific case of the aerial base stations, the uplink receiver has a wide field of view due to its high elevation and sees a large number of cochannel users (Figure 1.1). For these stations, the size and weight of the antenna array is an even more critical issue; it is very likely that the number of interferers exceeds the size of the array [Bay2000], and therefore spatial processing techniques can only partially cancel the cochannel interfering signals.

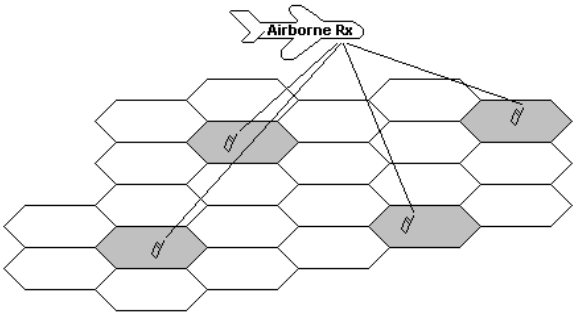

Figure 1.1 Airborne base stations; illustration of the CCI problem

From these considerations, it appears that the use of antenna arrays has not diminished the need for demodulation schemes robust to CCI. Actually, it is quite the opposite; by reducing the probability of receiving a large number of interferers (which can be accounted as noise), spatial processing has accentuated the need for specific demodulation schemes robust to a small number of interferers [Chi1996].

The goal of this work is to implement a non-coherent demodulation technique for minimum shift keying (MSK) modulation with improved performance in presence of CCI. With the success of the pan-European GSM system, MSK has become the most popular modulation format for narrowband cellular systems. By definition, 'cochannel' users are those who transmit simultaneously with identical carrier frequencies. However, for frequency shift keying (FSK) modulation, and particularly continuous phase FSK (which comprises MSK format), the instantaneous frequency of two cochannel signals also depends on the value of the transmitted symbols. Therefore, over a short observation interval the instantaneous frequency of the interferer may be different than that of the user of interest. Thus it may be advantageous to estimate the instantaneous frequency of the received signal with high resolution techniques; such an estimator could accurately estimate the dominant frequency of the received signal while rejecting the interference. In this thesis we have selected a specific frequency estimator and focused on the possible implementations of this model-based technique for the detection of MSK signals.

Chapter 2 of this thesis presents the MSK modulation format and some of the most common coherent and non-coherent demodulation schemes for MSK. In Chapter 3, parametric frequency estimation is introduced and a parametric technique is proposed for implementing an MSK detector. This model-based technique has been developed by Kumaresan and Tufts [Kum1982a] and was successfully applied to the demodulation of AMPS signals [Wel1996]. The implementation of this technique to MSK demodulation requires important modifications whose details are discussed in Chapter 4. The model-based scheme is combined with Viterbi equalization, evaluated in AWGN and Rayleigh fading environments and its performance is compared to the limiter-discriminator and the coherent Viterbi detector. Chapter 5 presents a study of the CCI rejection capabilities of the MSK demodulators. Demodulation diversity, first proposed for GMSK in [Las1997a], is investigated in conjunction with model-based detection. Finally, Chapter 6 concludes this thesis with a summary and some suggestions for future work.

Chapter 2 MSK Signals and Demodulation

Because of its attractive properties, continuous phase modulation (CPM) has seen wide usage in mobile communications. Minimum shift keying (MSK), which is a form of CPM, is the modulation format of several wireless standards such as the widely used pan European GSM (Global System for Mobile). MSK-type signals present a constant envelope, which permits the use of low complexity non-linear amplifiers and their low bandwidth spread limits adjacent-channel interference. This spectral efficiency can be further improved by appropriately pulse-shaping the data as in the case of Gaussian minimum shift keying (GMSK). Multiple demodulation schemes exist for CPM signals. When coherent detection is possible good bit-error performance may be achieved, whereas non-coherent schemes are easily implemented. A major characteristic of MSK is the inherent presence of inter-symbol interference (ISI) that limits performance of symbol-level detection schemes. Sequence estimators may be used to mitigate ISI at the price of increased complexity of the demodulation operation.

2.2 MSK Signals

Minimum shift keying is a special case of continuous-phase frequency shift keying (CPFSK). Similarly to frequency shift keying (FSK) the binary data is coded by two frequency tones, but the signal maintains a continuous phase between consecutive bits. This phase continuity property is the major reason for the higher bandwidth efficiency of CPFSK as compared to other FSK modulation formats.

The modulated waveform of a binary CPFSK signal with bit period T, carrier frequency f_c and bit energy E_b, may be expressed as [Skl1988][Pro2001]

$$s(t) = \sqrt{\frac{2E_b}{T}} \cos\left\{2p\left(f_c + a_n f_d\right)(t - nT) + j_n\right\} \qquad nT < t \le (n+1)T, \tag{2.1}$$

where j_n denotes the phase of the signal at time nT, which is the end of the previous bit. Also $\{a_n\}$ is a polar sequence of ± 1 that encodes the data. Depending on the current value of $\{a_n\}$, the frequency differs from its median value f_c by a quantity of ± f_d, called

the frequency deviation. As is obvious from equation (2.1), MSK signals have constant envelope and continuous phase, which are two major advantages of this modulation format.

The ratio of $2f_d$ (which is the spacing between the two frequency-tones f_c+f_d and f_c-f_d) to the bit rate is called modulation index and denoted h:

$$h = 2 f_d T \,. \tag{2.2}$$

The smaller the modulation index, the better is the spectral efficiency [And1986]. In the case of MSK, the modulation index is equal to 0.5. It is seen that this value for h is the minimum spacing for which the frequency tones are orthogonal when coherently detected [Skl1988][Pro2001]. However this minimum deviation does not insure orthogonal frequency tones when the phase is unknown.

The signal phase j_n at time nT, is the summation of the phase deviations of all previously transmitted symbols plus the initial phase j_0 of the carrier. Therefore, the phase of the baseband waveform can be expressed as [Pro2001]:

$$j_{LP}(t) = 2p\, f_d T \sum_{k=-\infty}^{n-1} a_k + 2p\, f_d\, a_n (t - nT) + j_0 \qquad nT < t \le (n+1)T \,, \tag{2.3}$$

which can be transformed into a more general expression, for all values of t:

$$j_{LP}(t) = 2p \int_{t=-\infty}^{t} f_i(t)\,dt + j_0 \,, \tag{2.4}$$

where $f_i(t)$ is defined as:

$$f_i(t) = f_d \sum_{k=-\infty}^{+\infty} a_k\, g(t - kT) \,, \tag{2.5}$$

and $g(t)$ is a rectangular pulse of amplitude one and duration T. Using (2.4) as the expression for the phase, the complex baseband waveform of MSK is:

$$v_{BB}(t) = \sqrt{\frac{E_b}{T}} \exp\left\{ j\left(2p \int_{t=-\infty}^{t} f_i(t)\,dt + j_0 \right) \right\}. \tag{2.6}$$

In signal processing, $f_i(t)$ is known as the instantaneous frequency of the signal at time t [Boa1992a]. In the case of MSK the instantaneous frequency of the baseband signal (2.5) is constant by parts, and equals $\pm f_d$ depending on the value of the current bit a_n.

A minimum shift keying signal can also be expressed in the form of an offset

quadrature phase shift-keying signal (OQPSK). As shown in [Ben1999] the previous expressions for the MSK waveform are equivalent to:

$$s(t)=\sqrt{\frac{2E_b}{T}}\left\{b_I(t)q\left(t-nT\right)\cos\left(2p\ f_c t+j_0\right)-b_Q(t)q\left(t-T-nT\right)\sin\left(2p\ f_c t+j_0\right)\right\}, \quad (2.7)$$

where

$$q(t)=\begin{cases}\cos\left(\dfrac{p\,t}{2T}\right), & -T\le t\le T\\ 0 & otherwise.\end{cases} \quad (2.8)$$

The real and imaginary parts of $s(t)$ carry the information on respectively the even numbered elements $\{b_{2n}\}$ and the odd numbered elements $\{b_{2n+1}\}$, where $\{b_n\}$ is the data stream to be transmitted. Namely, $b_Q(t)=b_{2n+1}$ for $2nT<t\le(2n+2)T$ whereas $b_I(t)=b_{2n}$ for $(2n-1)T<t\le(2n+1)T$. This representation of MSK as a form of OQPSK results in a simple implementation for the MSK modulator, with block diagram shown on Figure 2.1. Identification of the OQPSK representation (2.7) and CPFSK representation (2.1) for MSK gives the relationship between the data streams $\{a_n\}$ and $\{b_n\}$ as $a_n=b_nb_{n-1}$.

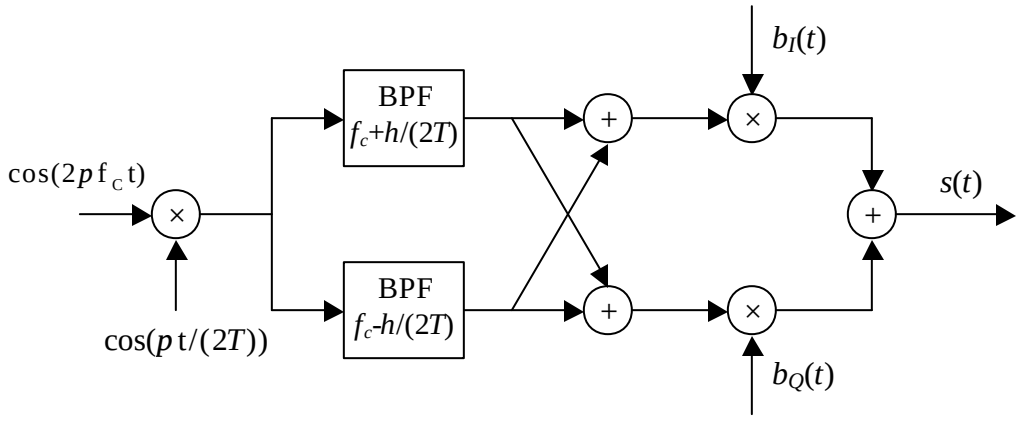

Figure 2.1 Block Diagram of an MSK transmitter [Rap1996]

2.2 Gaussian Pulse-Shaping for MSK

Gaussian minimum shift keying (GMSK) is a derivative of MSK with improved spectral efficiency. Prior to the modulation, the data sequence is shaped by a Gaussian filter $g(t)$. Then the modulation process is identical to MSK, as described in equations (2.5) and (2.6).

The Gaussian pulse shape has the form of:

$$g(t) = \left\{ Q\left(\frac{2\pi B}{\sqrt{\ln 2}} (t - \frac{T}{2}) \right) - Q\left(\frac{2\pi B}{\sqrt{\ln 2}} (t + \frac{T}{2}) \right) \right\}, \tag{2.9}$$

where the Q function is defined as

$$Q(t) = \int_t^{\infty} \frac{1}{\sqrt{2\pi}} e^{-\frac{x^2}{2}} dx . \tag{2.10}$$

The coefficient B sets the 3dB bandwidth of the pulse. The shapes of the Gaussian filtered pulses are plotted Figure 2.2 for different values of BT, the time-bandwidth product.

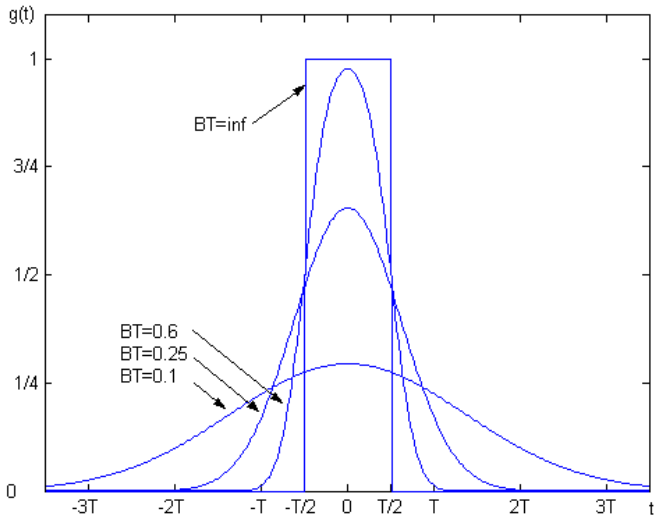

Figure 2.2 Gaussian shapes of GMSK pulses for four values of BT (BT=infinity corresponds to MSK)

Through the Gaussian filtering operation, the data stream is made continuous, and accordingly, the instantaneous frequency (2.5) of GMSK is continuous. The principal result of this is a power spectrum for GMSK that is more compact than for MSK. The power spectral density (PSD) of GMSK, with BT=0.25, is compared to the PSD for MSK and quaternary phase shift keying (QPSK) on Figure 2.3. The Gaussian shaping further compresses the spectrum of MSK, which is already a more efficient modulation format than QPSK. For GMSK (BT=0.25) 99.9% of the signal power is contained in a bandwidth of 1.09/T, whereas the bandwidth occupancy of MSK for the same amount of power is

2.76/*T* [Rap1996]. The Gaussian shaping attenuates the side-lobes of the spectrum, due to sharp frequency transitions within the MSK signal. The smaller the *BT* product chosen, the smoother are the frequency transitions, and the more compact is the GMSK spectrum. The spectral efficiency of MSK for different Gaussian and raised-cosine pulse-shapes is detailed in [And1986].

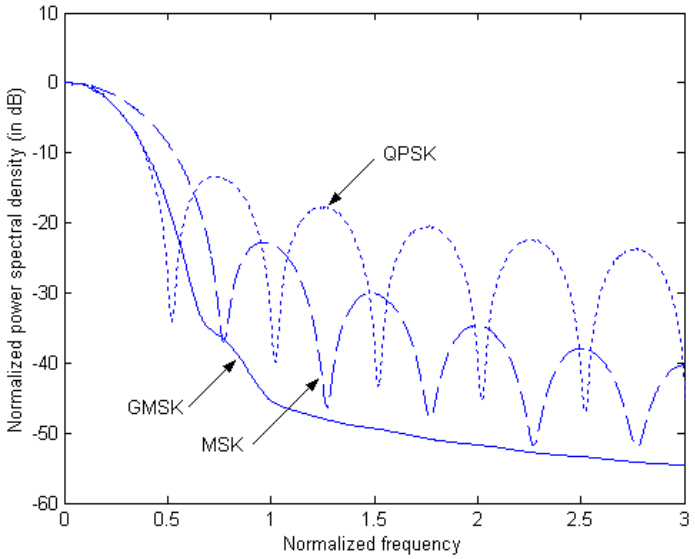

Figure 2.3 Estimated power spectral density for QPSK, MSK, and GMSK (*BT*=0.25)

Small values for *BT* are desirable to achieve good spectral efficiency; however long durations of the narrow bandwidth pulses result in large inter-symbol interference (ISI). Whereas MSK signals are full response (the duration of the rectangular pulse shape does not exceed *T*) GMSK signals are partial response, and consequently each symbol interferes with its surrounding neighbors. This inter-symbol interference increases for decreasing values of *BT*, and degrades the performance of simple demodulation schemes based on single symbol decision. GMSK modulation is used in the GSM standard with a time-bandwidth product equal to *BT*=0.3, and CDPD (Cellular Digital Packet Data) employs GMSK with *BT*=0.5. For what follows, the time-bandwidth product has been chosen as *BT*=0.25. As shown in Figure 2.2, for *BT*=0.25, the Gaussian pulse-shape is almost zero for $|t| > 1.5T$: the current symbol only affects the previous and next symbols. Therefore to ease the implementation of MSK modulation the pulse may be truncated

outside the time interval $[-1.5T;1.5T]$ with very little degradation of the spectrum [Pro2001].

The phase of the MSK signal is continuous between consecutive bits. As a result the signal has some memory of the past data bits. Gaussian pulse shaping further adds memory to the signal since it introduces ISI. Consequently single-symbol detectors for GMSK are outperformed by block and sequence estimation schemes. The eye diagram and phase trajectory of GMSK for a time-bandwidth product of 0.25 are shown Figure 2.4.a and 2.4.b. The effect of ISI is a reduction of the eye opening and an increase in the number of paths in the eye-diagram and in the phase tree as well.

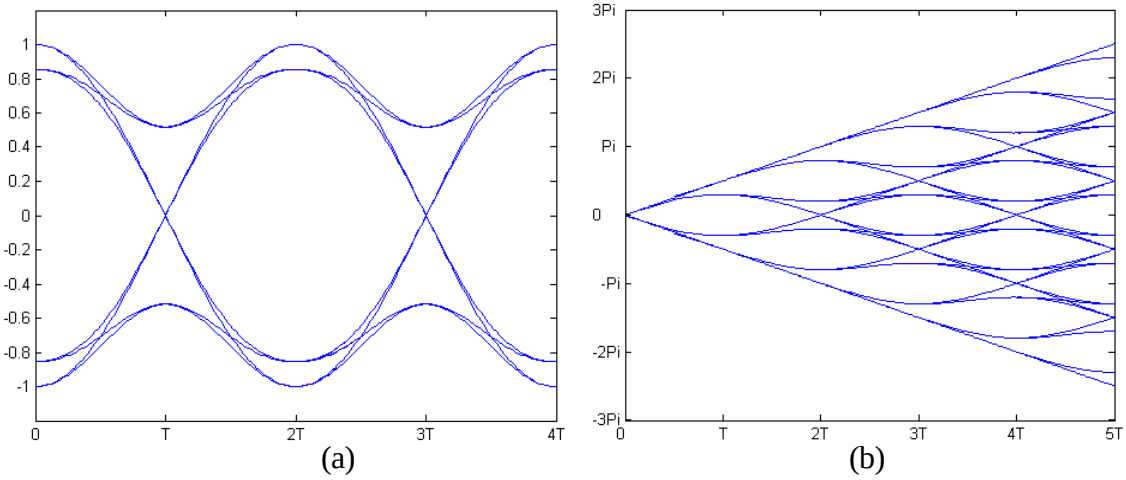

Figure 2.4 (a) Eye diagram and (b) phase trajectory for GMSK (BT=0.25)

Prior to detection, receivers for MSK and GMSK signals make use of an IF pre-detection filter that band limits the received signal and therefore reduces the input noise. The optimum IF filter depends on the shape of the MSK pulse and on the type of detection that follows the pre-detection filter. Whereas large values for the filter bandwidth B_{IF} will limit the ISI, the input noise power will be lower for small values of B_{IF}. For instance, in the case of GMSK signals with BT=0.25 and differential demodulation, it is shown in [Mur1981] and [Suz1981] that a Gaussian pre-detection filter with $B_{IF}T$=0.6 is nearly optimum.

2.3 Coherent Demodulation

When the carrier phase can be recovered at the receiver, good performance can be achieved with coherent demodulation. Minimum shift keying can be viewed as a special case of CPFSK with frequency deviation of h=0.5 or as a form of staggered QPSK with sinusoidal symbol pulse shaping weighting. These two representations motivate different structures for the demodulation.

First, the OQPSK representation of MSK may be employed to obtain a simple coherent demodulator. When seen as an OQPSK signal (2.7), the in-phase and quadrature parts of the MSK signal are independent and each one carries information of half of the original bit stream. The in-phase $I(t)$ and quadrature $Q(t)$ parts of the received signal $r(t)$ may be processed separately [Ben1999] (Figure 2.5). On the in-phase side, the coherent matched-filter is $q(-t)$ (2.8), whereas for the quadrature part the matched filter is $q(T-t)$. The output of the in-phase and quadrature matched filters are sampled at even and odd multiples of T, respectively.

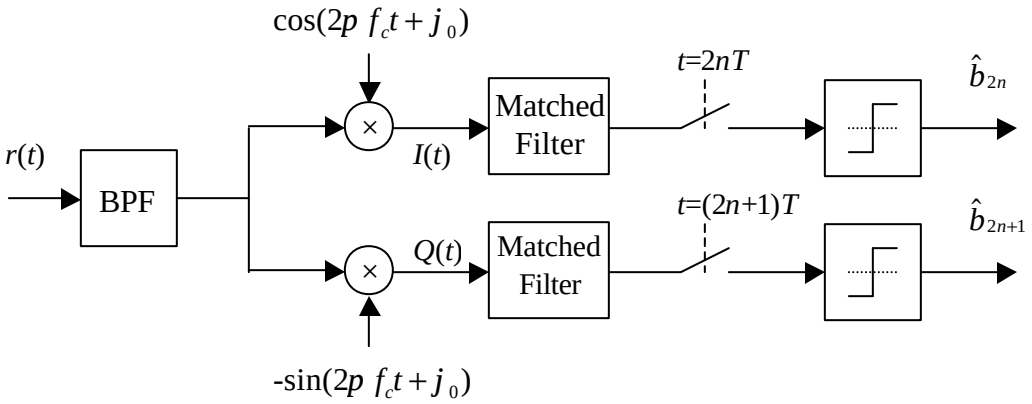

Figure 2.5 Block-diagram of a coherent demodulator for MSK [Las1997a]

An alternative coherent demodulation for MSK is the Viterbi detector. The MSK signal is now seen as a form of CPFSK (2.1). At time nT the phase of the baseband MSK signal can only take four values; and possible phase transitions are shown on the trellis diagram Figure 2.5.a. A phase shift of $+p/2$ corresponds to the transmission of the NRZ symbol +1, whereas symbol -1 results in a phase shift of $-p/2$. Under the assumption that the initial phase of the signal is zero, the MSK signal can also be represented by a two state tilted trellis diagram (Figure 2.6.b), where state 0 corresponds to the phase zero at

time t=0, $p/2$ at time T and so on, whereas state 1 has phase starting from p. The branch metrics for each of the four possible phase transitions $j_n(t, i \to j)$ between state $i \in \{0,1\}$ at time nT and state $j \in \{0,1\}$ at time $(n+1)T$ are calculated as [Pro2001]:

$$v_n(i \to j) = \int_{nT}^{(n+1)T} r(t)\cos\{2p f_c t + j_n(t, i \to j)\}dt . \qquad (2.11)$$

The Viterbi algorithm searches for the path through the trellis with minimum Euclidean distance from the received signal.

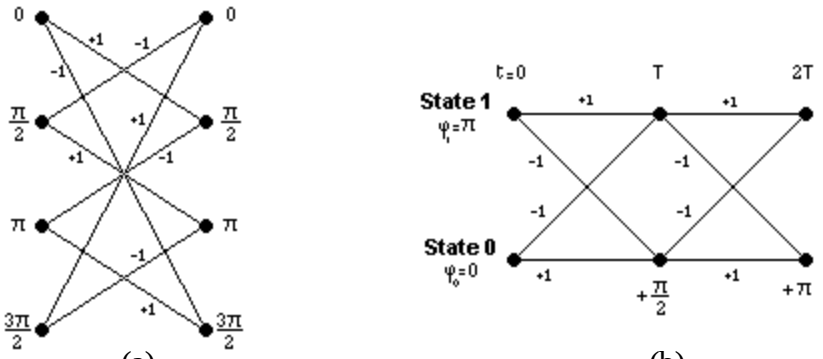

Figure 2.6 (a) Trellis diagram and (b) tilted-phase trellis diagram of MSK

The data sequence of MSK is oftentimes differentially encoded in order to prevent errors resulting from the possible 180° phase ambiguity in the carrier recovery. MSK with differential encoding is referred to as DMSK. Coherent receivers have been specifically developed for DMSK signals. Two of the most common implementations for DMSK are known as Massey's receiver and Rimoldi's receiver [Ben1999, Rim1988].

Offset matched filtering and Viterbi detection are both optimum maximum likelihood sequence estimators (MLSE) for MSK. Performance of MSK signals with optimum detection is similar to QPSK [Cou2001] and the bit-error probability is given in [Rap1996] as:

$$P_b = Q\left(\sqrt{1.7\frac{E_b}{N_o}}\right). \qquad (2.12)$$

A maximum likelihood sequence estimator based on the Viterbi algorithm can also be constructed for GMSK. However the number of states in the corresponding trellis is significantly increased: for a pulse-shape $g(t)$ having length LT the optimum Viterbi

receiver has 2^{L+1} states [And1986]. In [Mur1981] Murota and Hirade derived the expression for the bit-error probability of GMSK with coherent detection. For simplicity GMSK may be detected employing MSK-type coherent demodulators. Inter-symbol interference introduced by the pre-modulation filter reduces the performance by approximately 0.3dB relative to the optimum GMSK receiver [Lee1988].

2.4 Non-Coherent Demodulation

Although coherent receivers offer good performance, it is often preferred to avoid the complexity of the phase synchronization process, which requires the use of phase lock loops and is vulnerable to fading. As seen previously, when non-coherently demodulated, the frequency spacing of MSK tones is less that the minimum required for orthogonality. Therefore non-coherent techniques permit inexpensive demodulation of MSK signals, but with inferior performance in AWGN.

2.4.1 Differential Receiver

The first non-coherent receiver that we examine is the differential detector. Differential detection consists of comparing the phase of the signal at two different time instants. The interval between the two observations is usually a multiple of the bit-duration T, and most common receivers are one bit and two bit differential receivers, which means that the time-interval for phase comparison is T and $2T$, respectively. The general block diagram of a one-bit differential detector is shown Figure 2.7.

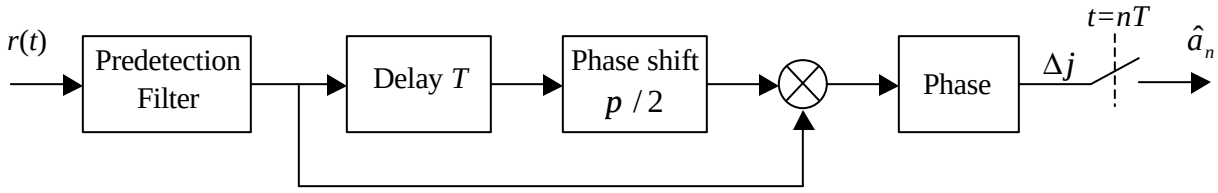

Figure 2.7 Block diagram of a differential detector

Using the complex baseband representation for the received signal and neglecting the effect of the IF filter, the expression for the differential phase is:

$$\Delta j\,(t) = \arg\{r_{BB}(t) r_{BB}{}^{*}(t-T)\} \tag{2.13}$$

This differential phase is sampled at time $t=nT$. From (2.5) the differential phase at time nT is given by

$$\Delta j\,(nT) = 2p \int_{t=(n-1)T}^{nT} f_d \sum_{k=-\infty}^{+\infty} a_k g(t-kT) + \Delta j_{noise}, \tag{2.14}$$

where Δj_{noise} corresponds to the effect of the additive noise. For MSK, the phase difference only depends on the value of the current bit, and the expression reduces to:

$$\Delta j\,(nT) = \frac{p}{2} a_n + \Delta j_{noise}. \tag{2.15}$$

In the case of GMSK with pulse-shape truncated for $|t| > 1.5T$, the decision statistic depends on three consecutive bits [Las1997a]:

$$\Delta j\,(nT) = \frac{p}{2}(a_{-1}a_{n-1} + a_0 a_n + a_{+1}a_{n+1}) + \Delta j_{noise}. \tag{2.16}$$

For BT = 0.25 the contributions of the three bits are weighted by a_0=0.589 and a_{-1}=a_{+1}=0.205.

Two bit differential detection is presented in [Sim1984]. The decision is made using the value of the difference between the signal phase at time t and t+2T. Two or three-bit differential detection have improved performances as compared to one-bit differential detection [Yon1988].

2.4.2 Discriminator Receiver

Similarly to frequency shift keying signals, MSK signals can be demodulated with limiter-discriminator receivers. The information content of the received signal is imbedded in its frequency, which is the derivative of the phase. This derivation can be performed employing a discriminator. The output of the discriminator is integrated over the bit duration T, for which the frequency is constant, and sampled at time $t=nT$. Finally, the decision statistic of the discriminator may be expressed similarly to (2.15) [And1986]. The block-diagram of the limiter-discriminator receiver is shown Figure 2.8. Prior to the discrimination operation, the signal is passed through a limiter that restores the constant envelop of the signal.

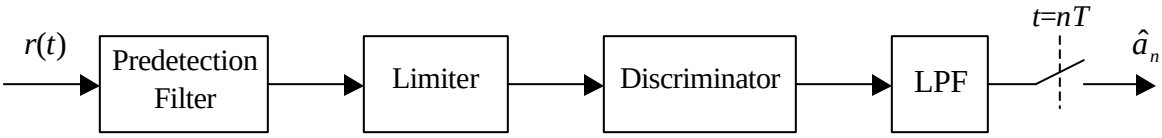

Figure 2.8 Block diagram of a limiter discriminator

For MSK (h=0.5), differential and discriminator detectors have identical performance in AWGN [Sim1983]. However, in the presence of co-channel interference, random FM noise or Rayleigh fading, the performance of differential detection and limiter discrimination slightly differ [Las1997a].

2.4.3 Non-Coherent Sequence Detection

The ease of implementation of non-coherent demodulators for MSK makes these techniques very attractive. However differential and limiter-discriminator detection suffer from the large ISI introduced by the IF pre-detection filter and also by the partial response pulse shaping for GMSK. Two approaches have been proposed to compensate this ISI. Hirono, Miki and Murota [Hir1984] developed a multilevel detection that employs decision feedback equalization (DFE). DFE may be used after a limiter-discriminator [Ada1988a] or with differential detection [Yon1988]. In both cases the output of the post-detection filter is corrected by the weighted values of the previously decided bits. Assuming that the SNR is large and that the pre-detection filter introduces no ISI, the decision statistic for GMSK after 1-bit differential detection and with 1-bit DFE can be written as:

$$\Delta j\,(nT) = \frac{p}{2}\left(a_{-1}\left\{a_{n-1} - \hat{a}_{n-1}\right\} + a_0 a_n + a_{+1} a_{n+1}\right) + \Delta j_{noise}. \qquad (2.17)$$

And if a_{n-1} has been correctly detected then

$$\Delta j\,(nT) = \frac{p}{2}\left(a_0 a_n + a_{+1} a_{n+1}\right) + \Delta j_{noise}. \qquad (2.18)$$

As compared to (2.16), the effect of the previous bit has been cancelled, and thus the demodulation suffers from only half of the original ISI. When the pulse spreads over more symbols, ISI from bits earlier than a_{n-1} can also be removed with 2-bit or 3-bit DFE.

The second method, proposed by Chung [Chu1984], makes use of post-detection maximum-likelihood sequence estimation (MLSE) or Viterbi detection. Since the noise at the output of the discriminator or the differential detector is not gaussian, a post-detection sequence estimation based on the Viterbi algorithm is not MLSE in the strict sense [Tun1994]. Also the non-Gaussian nature of noise at the input of the Viterbi detector prevents a rigorous analytical derivation of performance for the non-coherent sequence detector.

In [Chu1984], two-states trellises were first considered. Then Viterbi detectors for four states or more have been investigated to improve non-coherent detection [Iwa1995]. The eye-diagram of the signal at the output of the discriminator is shown in Figure 2.9 for BT=0.25 and $B_{IF}T$=0.6. The Gaussian pulse shape has length $3T$ and the IF filter has length $2T$. As a result the current symbol interferes only with the two previous and the two subsequent symbols [Iwa1995]. The memory of the signal at the input of the discriminator is L=5T, and the total number of possible paths is equal to 2^L=32; and the trellis diagram that represents all the transitions has 16 states. The block diagram of a non-coherent sequence detector with limiter discrimination is represented Figure 2.10.

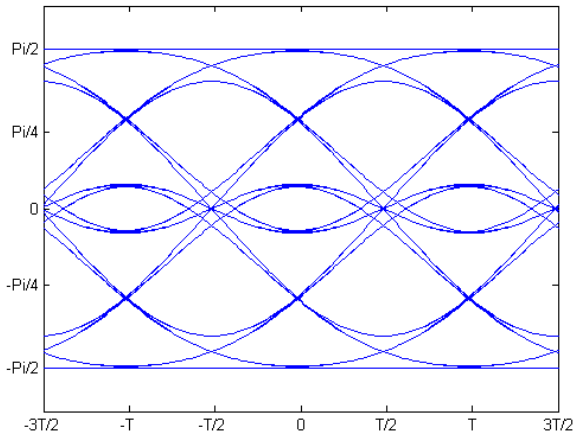

Figure 2.9 Eye pattern of the discriminator output for GMSK (BT=0.25) and Gaussian pre-detection filter ($B_{IF}T$=0.6)

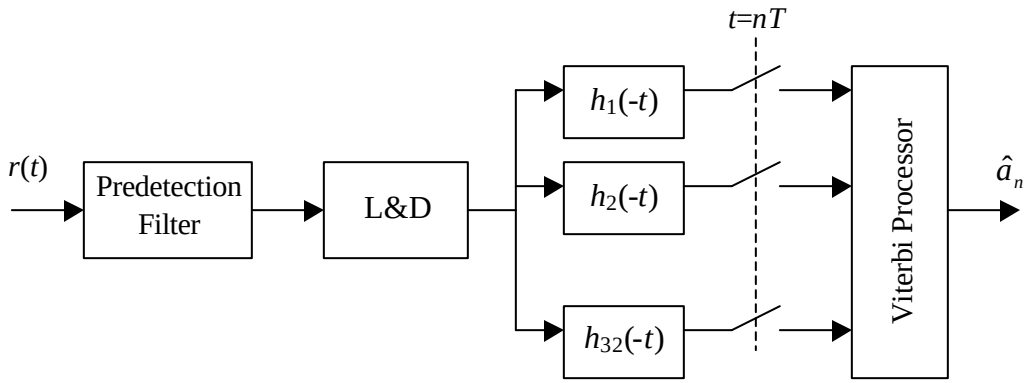

Figure 2.10 Block diagram of a sequence estimation scheme with limiter-discriminator detection.

Sequence estimation after the non-coherent detector diminishes the effect of ISI. Therefore IF filters with narrower bandwidth (and longer time duration) may be used to reduce the input noise, while ISI is compensated using augmented trellises [Iwa1995]. Large gains may thus be obtained with the non-coherent schemes, but with an increased complexity due to the large trellises employed in the sequence estimation process.

2.5 Summary

In this chapter, fundamentals of minimum shift keying signals have been presented along with some possible demodulation schemes. MSK is a form of frequency modulation. Coherent receiver mainly exploit the phase continuity property of MSK signals, while non-coherent receivers function by estimating the frequency of the signal and then comparing the estimate to a zero threshold. The conventional frequency detectors, such as the differential detector and the limiter-discriminator however, suffer from the small spacing between MSK frequency tones and have poor performance in noise corrupted environments. This limited performance is further degraded in the presence of co-channel interferers. As seen in Chapter 1, the capacity of a narrowband system is limited by co-channel interference. Therefore, robust performance in co-channel interference is a central matter, when choosing a demodulation scheme for MSK. In the next chapter improved frequency estimation techniques are investigated as possible substitutes to the differential detector and discriminator.

Chapter 3 Parametric Frequency Estimation

3.1 Overview on Frequency Estimation

Spectral estimation of a digital signal, and especially determination of its dominant frequencies is a major issue for a large number of communication problems. Frequency estimation techniques have been studied for use in speech processing, demodulation of analog FM signals and digital FSK signals, and for angle of arrival estimation in adaptive antenna arrays. When the purpose is to demodulate MSK signals in an interference-limited environment, the need is to find a spectral estimator that is able to distinguish between very closely spaced frequency tones and that precisely locates the peaks of the signal spectrum.

Spectral estimation techniques can be grouped into two categories: parametric techniques, also called model-based, and non-parametric techniques. Whereas non-parametric techniques make no assumption about the form of the signal, parametric estimators match the signal to a given model and make use of this model to estimate the signal spectrum. In addition to the classical Fourier analysis, the class of non-parametric techniques has recently been enriched with new time-frequency techniques such as the Wigner-Ville distribution [Boa1992b]. Meanwhile parametric techniques based on autoregressive modeling and subspace decomposition have been successfully applied to diverse applications.

The performance of the different techniques heavily depends on the type of signal that is to be estimated. This is even more obvious in the case of model-based techniques where performance relies on how closely the assumed model approximates the observed signal and where an inappropriate model could lead to irreducible error in the estimation. Parametric spectral estimation is a three steps process. First, a model for the signal is chosen. Then the model parameters are estimated such that the model accurately fits the observed signal. Finally the spectrum of the model is calculated and peaks of this spectrum are identified as the dominant frequency tones of the observed signal. Through the choice of a model, parametric techniques exploit some a-priori knowledge about the

signal structure. Therefore provided that the model is well chosen, parametric techniques can achieve higher accuracy than non-parametric techniques [Kay1988]. Typically for stationary signals a model-based technique can resolve frequency tones separated by only $1/(2N)$, where N is the number of data points available [Wel1996], which is twice better than resolution of the Fourier spectrum. For this reason parametric techniques are preferable to time-frequency analysis.

Among possible parametric techniques, rational spectral modeling techniques (and especially autoregressive modeling) are of prime interest due to their good performance and the ease of estimation of the model parameters. For the specific case of autoregressive frequency estimation, estimates of the parameters are typically found via linear prediction techniques. Moreover, accuracy of the autoregressive estimates can be significantly increased by taking advantage of the properties of the autocorrelation matrix eigen-decomposition [Kum1982b].

3.2 The Autoregressive Model

The choice of a good model for the observed signal is essential to ensure accurate frequency estimates. Techniques based on autoregressive (AR) modeling may successfully approximate peaks of the power spectrum for stationary signals [Kay1988]. Also as shown in Chapter 2, MSK signals have constant frequency over the duration of one bit. Therefore over a bit period, the signal received by a MSK base-station will mainly consist of one dominant frequency tone from the user of interest, white Gaussian noise, and possibly other interfering MSK signals resulting in some additional peaks in the power spectrum distribution. This received signal can be accurately modeled as an AR process.

An autoregressive process of order p is a linear stochastic process with outcome depending on the only p previous outcomes. If $x_{AR}(n)$ is an AR(p) signal then there exists a set of p coefficients $\{a_1,...,a_p\}$ such that:

$$x_{AR}(n) = \sum_{k=1}^{P} a_k \times x_{AR}(n-p) + w(n), \tag{3.1}$$

where $w(n)$ is a white Gaussian noise with variance s_W^2. AR signals can also be represented as the output of a linear filter with input white Gaussian noise $W(z)$ and transfer-function $H(z)$:

$$X_{AR}(z) = H(z)\,W(z). \tag{3.2}$$

Identification of equation (3.1) and (3.2) gives the expression for the transfer-function:

$$H(z) = \frac{1}{1-\sum_{k=1}^{p} a_k z^{-k}}. \tag{3.3}$$

The power spectral density $S_X(f)$ of the random process $x_{AR}(n)$ is defined as the Fourier transform of its autocorrelation function. If $x_{AR}(n)$ is given by (3.2) with $H(z)$ being a linear process, $S_X(f)$ can also be expressed as the product of the modulus of $H(z)$ squared and the power spectral density of the noise, which has amplitude s_W^2 [Clar1993]:

$$S_X(f) = S_W\left(e^{2\pi f}\right)\left|H\left(e^{2\pi f}\right)\right|^2 = \frac{s_w^2}{\left|1-\sum_{k=1}^{p} a_k e^{-2k\pi f}\right|^2}. \tag{3.4}$$

When an observed signal $x(n)$ is to be estimated via AR(p) modeling, the parameters $\{a_1,\ldots,a_p\}$ are chosen so that the AR model best represents the signal. Then an estimate of the power spectrum of the signal is given by (3.4). The noise power s_W^2 is constant over all frequencies and does not need to be estimated. Therefore the problem of estimating the power spectrum has been transformed into a problem of parameter estimation.

3.3 AR Parameter Estimation

3.3.1 Linear Prediction

The n^{th} sample of an autoregressive process linearly depends on its p previous values (3.1). Hence, for a complex sequence that may be modeled by an AR(p) signal, an estimate of its sample $x(n)$ can be found as a linear combination of $\{x(n\text{-}p),\ldots,x(n\text{-}1)\}$ using some weighting coefficients $\{c_1,\ldots,c_p\}$, called the prediction filter:

$$\hat{x}(n) = \sum_{k=1}^{P} c_k \times x(n-k). \tag{3.5}$$

The forward prediction differs from the observed value by the prediction error $e(n)$. This error $e(n)$ is a measure for the accuracy of the prediction.

$$e(n) = x(n) - \hat{x}(n) = x(n) - \sum_{k=1}^{P} c_k \times x(n-k) \tag{3.6}$$

Parametric estimation via linear prediction consists of finding the set of coefficients $\{c_1,\ldots,c_p\}$ such that the power of the prediction error is minimized. This is the least square solution for the linear prediction equation (3.5). If the signal is strictly AR and of same order of the prediction, then the AR parameters form a set of prediction coefficients with prediction error equal to $w(n)$ and error power s_W^2, which has been proved to be the minimum achievable power for the prediction error [Hay1996]. This is in contrast to the problem of parameter estimation where the true AR coefficients are unknown but approximated by the least square solution of the linear prediction problem.

At this point it might be helpful to consider the noiseless case, where the signal of interest is only composed of *M* complex sinusoids. It is easily shown that such a signal can be exactly predicted with a prediction filter of order p equal to *M*. For instance a single sinusoid of frequency f_1 will yield a next sample equal to its current value but with phase shifted by $2p\,f_1$: in other words $c_1 = \exp(j2p\,f_1)$. In the case of two complex sinusoids with normalized frequencies f_1 and f_2, the second order prediction coefficients can be found as $c_1 = \exp(j2p\,f_1) + \exp(j2p\,f_2)$ and $c_2 = -\exp(j2p\,(f_1 + f_2))$ with zero prediction error. However, in the noisy case a prediction with order equal to the number of pure sinusoids present in the signal is not always desirable. The presence of noise at a high level can be attributed to an increase in the signal complexity and consequently linear prediction of order higher than *M* may describe the signal more accurately.

3.2.2 Yule-Walker Equations

The general least square (LS) solution for the linear prediction problem is derived in this section. Following (3.3) the average power of the prediction error can be written as

$$P_e = E\left\{\left|e(n)\right|^2\right\} = E\left\{\left|x(n) - \sum_{k=1}^{P} c_k \times x(n-k)\right|^2\right\}. \tag{3.7}$$

Introducing the autocorrelation function $r_{XX}(k)$, another expression for this mean square prediction error is

$$P_e = r_{XX}(0) - r_{XX}{}^H c - c^H r_{XX} + c^H R_{XX} c\,, \tag{3.8}$$

where the autocorrelation function is defined for k ranging from 0 to p as

$$r_{XX}(k) = E\{x(n)x^*(n+k)\}\,, \tag{3.9}$$

and the autocorrelation matrix and autocorrelation vector have the form of respectively

$$R_{XX} = \begin{bmatrix} r_{XX}(0) & r_{XX}^*(1) & \cdots & r_{XX}^*(p-1) \\ r_{XX}(1) & r_{XX}(0) & \cdots & r_{XX}^*(p-2) \\ \vdots & \vdots & \ddots & \vdots \\ r_{XX}(p-1) & r_{XX}(p-2) & \cdots & r_{XX}(0) \end{bmatrix}, \qquad r_{XX} = \begin{bmatrix} r_{XX}(1) \\ r_{XX}(2) \\ \vdots \\ r_{XX}(p) \end{bmatrix}. \tag{3.10}$$

After differentiation of equation (3.8) with respect to the complex vector c of prediction coefficients, the minimum prediction error power is found by setting $\frac{\partial P_e}{\partial c} = 0$, which is equivalent to [Vas2000]:

$$R_{XX} c - r_{XX} = 0\,. \tag{3.11}$$

This relation between the least square prediction coefficients and the autocorrelation function is the matrix form of the Yule-Walker equations for AR modeling [Kay1988]. When R_{XX} is invertible, the solution for the Yule-Walker equations is simply

$$c = R_{XX}{}^{-1} r_{XX}\,. \tag{3.12}$$

Since the true autocorrelation function of the signal is unknown, $r_{XX}(k)$ (3.9) must be estimated from the available samples. As a consequence, the general least-square solution in (3.12) leads to several parametric methods, depending on the choice for the approximation of the autocorrelation function.

A simple approximation of $r_{XX}(k)$ is given by the following expression:

$$r_{XX}(k) = \frac{1}{N} \sum_{n=1}^{N} x(n)x^*(n+k)\,, \tag{3.13}$$

where $x(n)$ is assumed to be zero outside the observation interval. The resulting AR model is called the autocorrelation method. Due to its relatively poor spectral estimation other AR techniques described below are usually preferred to the autocorrelation method.

3.3.3 Covariance Method

If a total of $N>p$ consecutive data samples are available, then $N-p$ forward prediction equations analogous to (3.6) can be written. Also, as the observed signal is assumed to be stationary over those N samples, the prediction coefficients are unchanged for these $N-p$ equations. The resulting set of equation can be written in matrix form:

$$\underbrace{\begin{bmatrix} e(1) \\ e(2) \\ \vdots \\ e(N-p) \end{bmatrix}}_{e} = \underbrace{\begin{bmatrix} x(p+1) \\ x(p+2) \\ \vdots \\ x(N) \end{bmatrix}}_{x} - \underbrace{\begin{bmatrix} x(p) & x(p-1) & \cdots & x(1) \\ x(p+1) & x(p) & \cdots & x(2) \\ \vdots & \vdots & \ddots & \vdots \\ x(N-1) & x(N-2) & \cdots & x(N-p) \end{bmatrix}}_{X} \underbrace{\begin{bmatrix} c_1 \\ c_2 \\ \vdots \\ c_p \end{bmatrix}}_{c}. \tag{3.14}$$

As seen above, a good prediction should result in an estimate with minimum average error power. If P_e is the mean power of the $N-p$ forward prediction errors then

$$P_e = \frac{1}{N-p} e^H e = \frac{1}{N-p}\left(x^H x - x^H X c - c^H X^H x + c^H X^H X c\right). \tag{3.15}$$

When $X^H X$ is invertible, the minimum of P_e is found when [Sto1997]

$$c = X^+ x = \left(X^H X\right)^{-1}\left(X^H x\right), \tag{3.16}$$

with X^+ defined as the pseudo-inverse or Moore-Penrose generalized inverse of X. This least square solution for the AR model parameters is often referred to as the forward-prediction solution, the covariance method or extended Prony's method. Replacing the autocorrelation matrix R_{XX} and autocorrelation vector r_{XX} by respectively $X^H X$ and $X^H x$, then the covariance method (3.16) represents an approximate solution for the Yule-Walker problem (3.12), and an alternative to the autocorrelation method.

Resulting from their similarity, the autocorrelation and covariance methods have comparable performance for large values of N. However, for a smaller number of samples, the autocorrelation and covariance methods have a slightly different behavior [Sto1997]. In the case of the modified covariance method, the AR model parameters

obtained may be unstable, whereas the autocorrelation method insures the stability of the model. Yet unstable AR parameters are very unlikely and, what is more, stability is not an issue for the frequency estimation problem..

Also for small values of N, the covariance method is seen to outperform the autocorrelation method. The underlying assumption made by the autocorrelation method is that the signal equals zero outside the observation interval [Hay1996]. This incorrect assumption results in end effects and degrades the performance when the number of samples N is small. From equation (3.13) the function $r_{XX}(k)$, $k=\{0,\ldots,N\text{-}1\}$, is averaged over N lag products for the autocorrelation method, k of which are zero [Kay1988]. Consequently the estimated autocorrelation function may become unreliable for k close to N. By contrast the covariance method estimates each autocorrelation value $r_{XX}(k)$, $k=\{0,\ldots,N\text{-}p\}$ as the mean of a constant number of p measurements, making no assumption for the signal outside the observation interval. Yet for k close to zero the covariance method does not employ all possible N-k lag products to estimate the autocorrelation function, which is the case for the autocorrelation method and also for the modified covariance method.

3.3.4 Modified Covariance Method

Forward prediction consists of predicting the sample x(n) from the p previous observations $\{x(n\text{-}p),\ldots,x(n\text{-}1)\}$. Alternatively, if $\{x(n+1),\ldots,x(n+p)\}$ are known it may be possible to guess the value of the previous data sample $x(n)$; this procedure is called backward prediction. While prediction of the past may not seem very pertinent, backward prediction is of great help when the purpose is to estimate the AR parameters of a signal. The backward linear prediction of $x(n)$ with prediction coefficients $\{b_1,\ldots,b_p\}$may be expressed as:

$$\hat{x}(n) = \sum_{k=1}^{P} b_k \times x(n+k) \,. \tag{3.17}$$

The forward (3.5) and backward (3.17) linear predictions are similar except that the data coefficients are reversed in time. As a result, the optimum solution for the backward vector coefficients $\{b_1,\ldots,b_p\}$ is directly related to the optimum forward

coefficients $\{c_1,\ldots,c_p\}$ and more precisely $\{c_1,\ldots,c_p\}$ is the complex conjugate of the reversed backward filter $\{b_p,\ldots,b_1\}$ [Kay1988].

While $(N\text{-}p)$ equations for the forward prediction error were written in (3.14), an additional set of $(N\text{-}p)$ backward equations can be derived from N samples when the order of prediction is p. The combination of the $2(N\text{-}p)$ equations gives:

$$\underbrace{\begin{bmatrix} e_F(1) \\ e_F(2) \\ \vdots \\ e_F(N-p) \\ e_B(1) \\ e_B(2) \\ \vdots \\ e_B(N-p) \end{bmatrix}}_{e_{FBLP}} = \underbrace{\begin{bmatrix} x(p+1) \\ x(p+2) \\ \vdots \\ x(N) \\ x^*(1) \\ x^*(2) \\ \vdots \\ x^*(N-p) \end{bmatrix}}_{x_{FBLP}} - \underbrace{\begin{bmatrix} x(p) & x(p-1) & \cdots & x(1) \\ x(p-1) & x(p) & \cdots & x(2) \\ \vdots & \vdots & \ddots & \vdots \\ x(N-1) & x(N-2) & \cdots & x(N-p) \\ x^*(2) & x^*(3) & \cdots & x^*(p+1) \\ x^*(3) & x^*(4) & \cdots & x^*(p+2) \\ \vdots & \vdots & \ddots & \vdots \\ x^*(N-p+1) & x^*(N-p+2) & \cdots & x^*(N) \end{bmatrix}}_{X_{FBLP}} \begin{bmatrix} c_1 \\ c_2 \\ \vdots \\ c_p \end{bmatrix} \quad (3.18)$$

The solution that minimizes the power of the total prediction error e_{FBLP} is identical to the covariance method (3.16) except that data vector x and data matrix X are now of respective dimensions $2(N\text{-}p)$ and $2(N\text{-}p)\times p$ as defined above (3.18). This procedure is called the modified covariance or forward-backward method [The1992]. Solving for the model parameters by way of the modified covariance method minimizes the sum of the forward and backward error power and leads to a significant increase in performance. As the autocorrelation function is averaged over a number of lag products larger than the initial covariance method, variance of the estimated parameters is reduced.

Frequency estimates obtained from the modified covariance method present various advantages such as a relatively low bias, a small dependence on the initial phase and a high resolution at moderate SNR [Kay1988]. This makes the modified covariance a good candidate for the present application. However, the performance of this method degrades for low SNR, which motivates the use of advanced noise reduction techniques.

3.4 Subspace Decomposition of the Autocorrelation Matrix

3.4.1 Properties of the Autocorrelation Matrix

Each of the AR modeling techniques presented above relies on an estimate of the autocorrelation matrix. For reasonable signal to noise ratio this estimate is accurate and parameters precisely fit the signal. However, when the noise power is high the resulting autocorrelation matrix and prediction filter may contain a large portion of the noise. To attenuate the effect of noise and improve the AR methods, subspace decomposition is performed on the autocorrelation matrix.

The use of subspace decomposition of the autocorrelation matrix for frequency estimation was initially employed in the Pisarenko Harmonic Decomposition [Kay1988]. This technique has been improved to give the Multiple Signal Classification method (MUSIC) and more recently the Estimation of Signal Parameters via Rotational Invariance techniques (ESPRIT) [The1992]. In these techniques, eigenvalue decomposition of the autocorrelation matrix is performed to determine directions of the signal and noise spaces. In the case of AR modeling, the eigenvalue decomposition may be used as a noise reduction technique for the autocorrelation matrix [Kum1982a].

For a signal composed of M frequency tones with additive white Gaussian noise it can be shown that the theoretical $L \times L$ autocorrelation matrix is the summation of a signal autocorrelation matrix and a noise autocorrelation matrix with the following properties [Kay1988]. The first matrix has rank M. Each of its M non-zero eigenvalues is equal to the power of one of the M sinusoids. The corresponding M eigenvectors span the signal space. The second matrix is full rank and its L eigenvalues are equal to the noise power s_W^2. The result is a total autocorrelation matrix that has M principal eigenvalues $\{ l_1,..., l_M \}$ and a remaining L-M almost zero eigenvalues $\{ l_{M+1},..., l_L \}$. Moreover, the noise space spanned by the L-M eigenvectors $\{e_{M+1},\ldots,e_L\}$ corresponding to the L-M smallest eigenvalues is orthogonal to the signal space [The1992].

With these notations the eigen-decomposition of the autocorrelation matrix is:

$$R_{XX} = \sum_{i=1}^{L} l_i e_i e_i^H = \underbrace{\sum_{i=1}^{M} l_i e_i e_i^H}_{signal\ space} + \underbrace{\sum_{i=M+1}^{L} l_i e_i e_i^H}_{noise space} . \qquad (3.19)$$

As the noise space is orthogonal to the signal space and consequently does not contain any relevant information on the signal, the autocorrelation matrix can be approximated as

$$\hat{R}_{XX} = \sum_{i=1}^{M} l_i e_i e_i^H . \tag{3.20}$$

This reduced rank approximation of the autocorrelation matrix will then be used instead of the original autocorrelation matrix to estimate the AR parameters in (3.12). The overall effect of this subspace technique is a decrease in the noise power of the estimated parameters. Consequently at low SNR much higher frequency resolution can be achieved as compared to the simple linear prediction techniques.

3.4.2 Kumaresan and Tufts's Method

Work performed by Kumaresan and Tufts has contributed to the improvement of the modified covariance method [Kum1982a][Kum1982b] through an efficient method to combine forward-backward linear prediction and the principal component approach.

Recall that the modified covariance method minimizes the sum of the forward and backward prediction errors and estimates the autocorrelation matrix by $R_{XX}=X^HX$, where X is defined as in equation (3.18). For further improvement of the modified covariance method, R_{XX} can be replaced by its reduced rank approximation containing only M dominant components. The principal component of the $p\times p$ autocorrelation matrix may be obtained by eigenvalue decomposition. But for large values of prediction order, computation of the principal components via eigen-decomposition may become impractical. However Kumaresan and Tufts have shown that this complex decomposition of the autocorrelation matrix can be avoided and replaced by a simpler operation on the data matrix X while preserving the advantages of subspace decomposition [Kum1982b].

For the $2(N\text{-}p)\times p$ data matrix X the ordinary singular value decomposition (SVD) is the factorization of X into three matrices U, Σ and V such that [Jen1991]

$$X = U\Sigma V^H , \tag{3.21}$$

and where Σ is a $2(N\text{-}p)\times p$ diagonal matrix with diagonal elements s_i known as the singular values of X. Then X^HX can be expressed as

$$X^H X = (U\Sigma V^H)^H U\Sigma V^H = V|\Sigma|^2 V^H . \tag{3.22}$$

Identification of the expressions for $X^H X$ in (3.22) and R_{XX} in (3.19) leads to the conclusion that the eigenvalues of the autocorrelation matrix are simply the norm squared of the singular values of X. Therefore there is a one to one correspondence between the principal components of R_{XX} and the principal singular values of X, and rank reduction of the autocorrelation matrix is equivalent to rank reduction of the data matrix X,

$$\widehat{X} = \sum_{i=1}^{M} s_i u_i v_i^H . \tag{3.23}$$

The solution for the AR parameters may be obtained by multiplying the pseudo inverse of X by the data vector x (3.16). Using the singular value decomposition of X, it is seen that the pseudo-inverse X^+ is equal to [Jen1991]:

$$X^+ = \left(X^H X\right)^{-1} X^H = V \Sigma^+ U^H . \tag{3.24}$$

The pseudo-invert of Σ is a $p \times 2(N-p)$ diagonal matrix with diagonal elements s_i^+ equal to s_i^{-1} if s_i is non-zero or zero otherwise. If the data matrix is replaced by its reduced rank approximation (3.23), the only M dominant singular values are kept and the pseudo-inverse X^+ is approximated as

$$\widehat{X}^+ = \sum_{i=1}^{M} \frac{1}{s_i} v_i u_i^H . \tag{3.25}$$

In summary Kumaresan and Tufts's method estimates the AR parameters as [Kum1982a]

$$\hat{c} = \widehat{X}^+ x = \sum_{i=1}^{M} \frac{1}{s_i} v_i u_i^H x . \tag{3.26}$$

Specifically, when the signal of interest is a simple sinusoid imbedded in white Gaussian noise, the principal component AR estimator consists in

$$c_{PC} = \frac{1}{s_1} v_1 u_1^H x . \tag{3.27}$$

With Kumaresan and Tufts's method, computation of the eigen-decomposition of the $p \times p$ autocorrelation matrix is replaced by a singular value decomposition of the $2(N-p) \times p$ data matrix X, which for practical values of p may save a significant amount of computation while fully exploiting the subspace decomposition.

3.5 Frequency Estimation by AR Modeling

3.5.1 Polynomial Rooting

Linear prediction and eigenvalue-decomposition techniques have been reviewed as a mean to estimate the AR parameters. One of the motivations for obtaining the AR(p) parameters is to analyze the direct relationship between these parameters and the spectrum of the autoregressive signal. From (3.4), an estimate of the observed signal spectrum is, within a multiplicative constant, the magnitude of the frequency response of filter $H(z)$, where the true AR parameters $\{a_1,\ldots,a_p\}$ are now replaced by their estimates $\{c_1,\ldots,c_p\}$.

The observed signal is assumed to be composed of M pure sinusoids, which are to be estimated, and additive noise. Provided that the power of these sinusoids is high enough compared to the noise level, frequency components of the signal will result in peaks in the estimated power spectrum. To get the frequency of these peaks, the response of $H(z)$ can be evaluated for a fine grid of frequencies. Then the M local maximums with highest power are chosen as estimates for the frequency components. To obtain good accuracy for the peak location, the frequency response of $H(z)$ must be computed for a large number of points; therefore precise estimation of the components requires numerous calculations.

Polynomial rooting is an alternative method for estimating the frequency components, that is sometimes less computationally intensive. Peaks of the spectrum are found when the polynomial denominator of $H(z)$ is close to zero. Therefore there is a direct correspondence between the roots of the polynomial $\{1,-c_1,\ldots,-c_p\}$ and peaks of the filter response. In the complex plane, the angle of the poles corresponds to the peak frequencies of the spectrum and closeness of the poles to the unit circle gives an estimate of the magnitude of the spectrum at these frequencies. The correspondence between the location of the poles and the peak frequencies of the power spectrum is clearly seen by comparison of the normalized frequency response of the digital filter $H(z)$ (Figure 3.1.a) with position of its nine poles (Figure 3.1.a), obtained for a signal composed of four sinusoids in AWGN. Angles of the poles have been represented as vertical lines in the power spectrum plot (Figure 3.1.a) and perfectly match the position of the peaks.

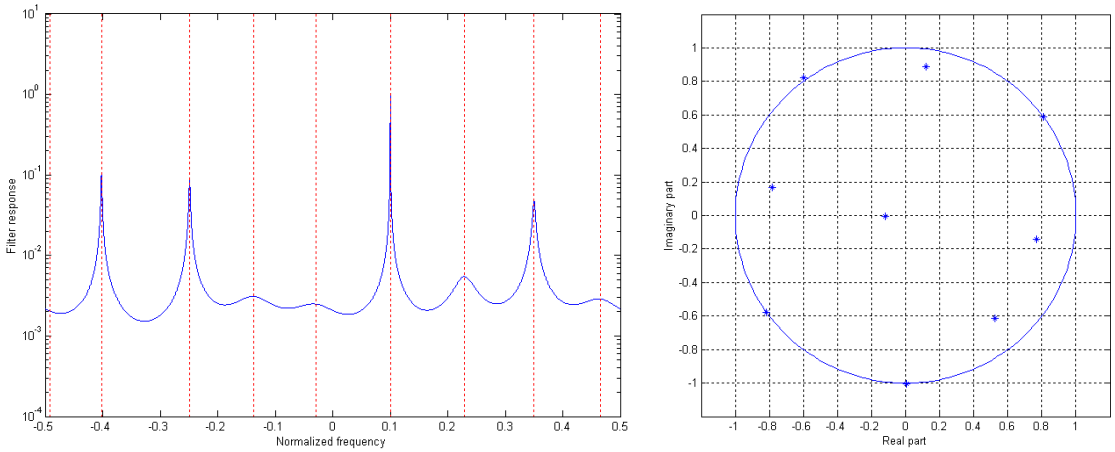

Figure 3.1 (a) Estimated AR spectrum and (b) location of the nine roots of the filter denominator obtained for a signal composed of four sinusoids in AWGN

Thus frequency estimates of the M sinusoids may either be chosen as the peak of the estimated spectrum or, equivalently, as the angles of the M poles closest to the unit circle, obtained by finding the roots of $\{1,-c_1,\ldots,-c_p\}$. Moreover the pole-zero plot gives a convenient visualization of the effect of the different AR techniques, and in particular it provides some insight for the choice of the model order.

3.5.2 Model Order Selection

The choice of an efficient parametric method is important, and accuracy of the frequency estimate will primarily depend on the selection of an appropriate order p for the AR model. It was previously seen that for a noiseless signal a prediction order equal to the number M of sinusoids present is sufficient. However, when noise becomes significant, M is no longer the optimum value for the prediction order p.

To illustrate the effect of noise, a signal composed of two equal-power complex sinusoids is considered. The two sinusoids have initial phase equal to zero and normalized frequencies centered on zero and spacing of $1/2N$, with N equal to 25. The signal is corrupted by additive white Gaussian noise. Pole locations obtained for multiple trials of the modified covariance method are shown on Figure 3.2.a for a model order of $p=M=2$ and Figure 3.2.b for $p=8$. These figures show that the separation of the two frequency tones is not possible when p and M are equal. Actually, in the case $p=M$, one of

the two poles is approximately located on the unit circle and corresponds to the sinusoids, whereas the other pole is inside the unit circle and represents the noise. On the other hand the use of a higher model order enables distinction between the two tones (Figure 3.2.b). The drawback to increasing the model order is the presence of p-M noise poles with position possibly close to the unit circle, which may be interpreted as signal poles. Therefore for the modified covariance method, the choice of the model order p results in a trade-off between the frequency resolution and the probability of occurrence of spurious peaks in the estimated spectrum. It has been shown that values of p that offer the best trade-off are between $N/3$ and $N/2$ [Kay1988][Kum1982b].

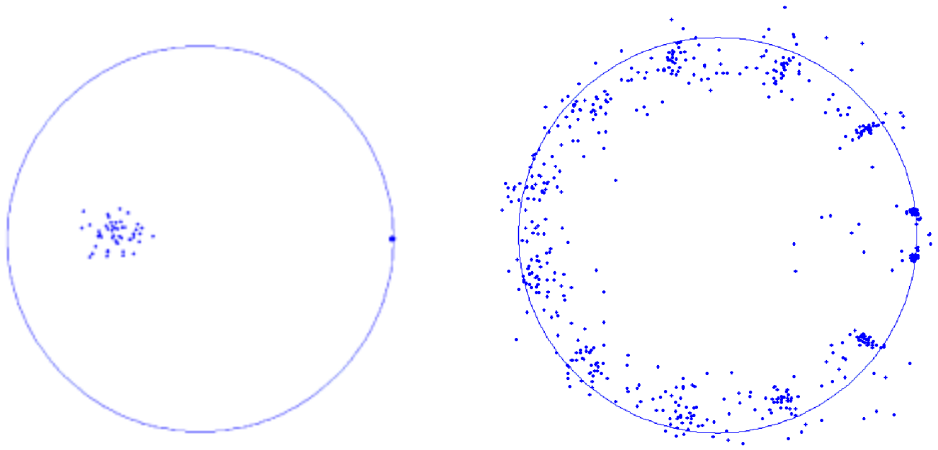

(a) (b)

Figure 3.2 Pole locations obtained for two complex sinusoids in AWGN with multiple trials of the modified covariance with order (a) $p = 2$ and (b) $p = 12$

For reasonable SNR, good frequency resolution can be achieved by the modified covariance method. But when the noise power is increased, the positions of the noise poles get closer to the unit circle and may result in erroneous frequency estimates. Kumaresan and Tuft's proposed method employs only the M principal components of the data matrix in the covariance method to mitigate the effect of noise. For a signal composed of two sinusoids as previously described but with a data record of length N equal to 12 and a prediction order p=9, the spectrum and pole locations obtained by the modified covariance method are compared to the results for the Kumaresan and Tufts's method (Figure 3.3). In this case, Kumaresan and Tufts's method approximates the autocorrelation matrix with its two principal components. One effect of this noise

reduction is the disappearance of the spurious peaks in the estimated spectrum, and accordingly, noise poles get more distant from the unit circle in the pole-zero plot. The chance of misinterpreting a noise pole as a signal pole is thus reduced while the frequency resolution is increased, because the order of the model can be higher than for the modified covariance method.

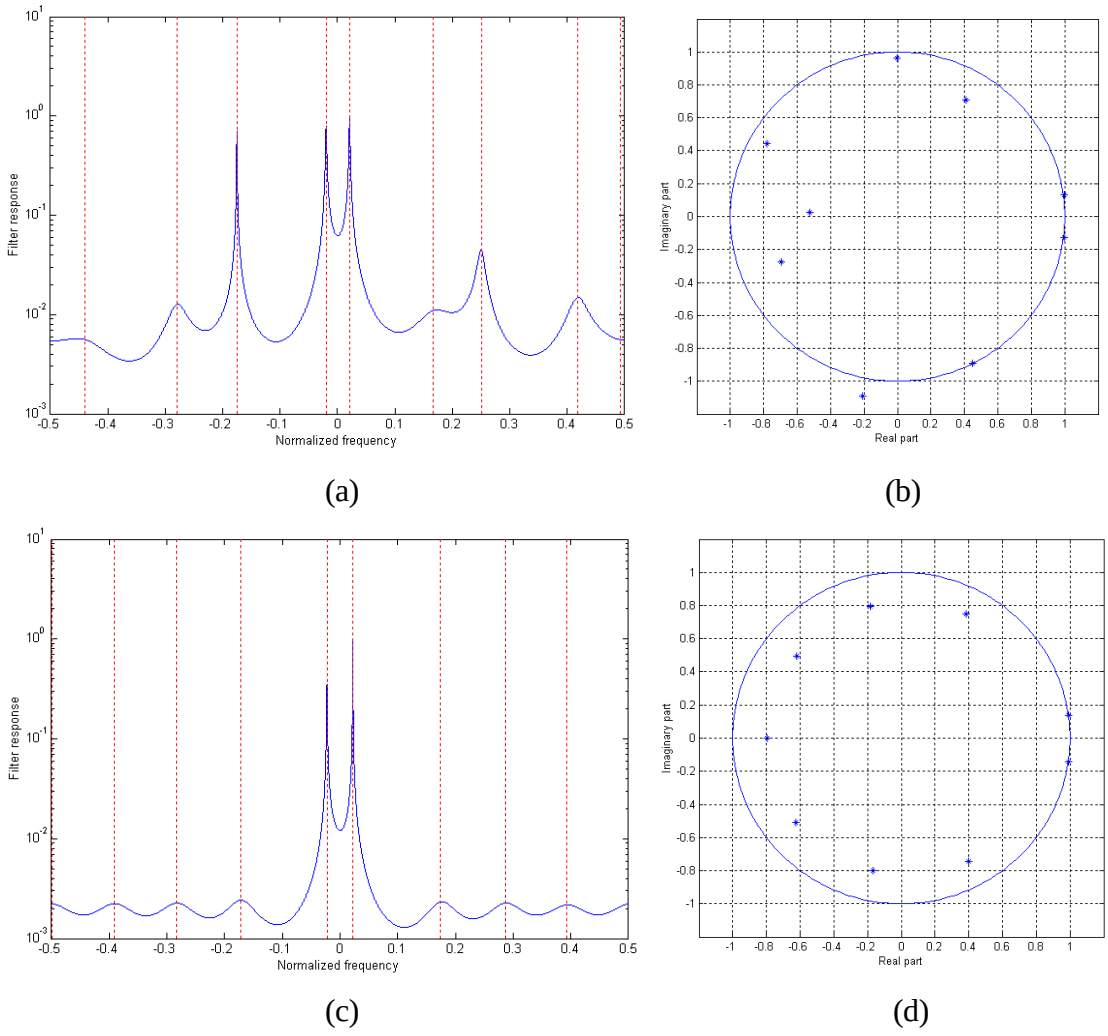

Figure 3.3 Comparison of the estimated spectrum and pole locations obtained for two complex sinusoids in AWGN with (a,b) the forward-backward autocorrelation matrix and (c,d) its reduced-rank approximation (two principal components). N=12 and p=9.

The optimum value for p was experimentally found to be $3N/4$ [Kum1982b], whereas the number of components selected in the SVD decomposition depends on M. Although the number of sinusoids present in the signal may not be exactly known in

practice, in many cases of interest only one or two dominant components are of interest and other sinusoids will have lower power. Therefore in most cases the only one or two principal components are kept, no matter what the number of interfering sinusoids may be.

3.6 Summary

In this chapter some high-resolution frequency estimation techniques have been presented as possible candidates for implementation as a minimum shift keying demodulator. As minimum shift keying is a form of frequency modulation (with continuous phase) the received signal may be detected based on the estimation of its instantaneous frequency. However, due to the minimum frequency deviation of MSK, only high-resolution estimators, such as the autoregressive frequency estimators, are of interest.

AR modeling leads to the Yule-Walker equations. The autocorrelation, the covariance and the modified covariance methods are alternative solutions for this problem. Then the properties of the eigen-decomposition of the autocorrelation matrix and their applications to noise reduction have been overviewed. Finally two techniques were presented to obtain the instantaneous frequency of the signal from the estimated AR parameters.

Kumaresan and Tufts principal component approach combines parametric modeling and subspace decomposition. The advantages of this method are its low bias, similarly to the modified covariance method, a good resistance to noise due to the subspace decomposition, and a reasonable complexity, resulting from the decomposition of the data matrix rather than the autocorrelation matrix.

A non-coherent demodulator for MSK signals must be able to distinguish between two frequency tones with spacing $f_S/(2N)$. Also, in presence of co-channel interferers, the demodulation of the strong signal requires further accuracy of the spectral estimator. These considerations have motivated our choice to implement a MSK demodulator based on the principal component method developed by Kumaresan and Tufts [Kum1982b].

Chapter 4 Implementation of a Model Based Demodulator

Parametric frequency estimation has been proposed in [Wel1996] as a demodulation technique for the Advanced Mobile Phone System (AMPS). AMPS signals are frequency modulated; therefore the demodulation of AMPS signals is a frequency estimation problem. In particular, the principal component technique, as presented in Chapter 3, is shown in [Wel1996] to offer good performance as a demodulator for AMPS and to be robust to co-channel interference. Those results have motivated our choice to adapt this frequency estimation technique to the demodulation of digital FM signals, and especially of MSK-types signals.

The implementation of a model-based (MB) demodulator to detect MSK signals is investigated in this chapter. First, a simple demodulation scheme based on Kumaresan and Tufts method is proposed for the detection. Exploiting a-priori information on the form of the received signal, and employing pre-detection filtering and post-detection sequence estimation, the performance of this model-based scheme can be significantly enhanced. Finally, the performance of the improved model-based demodulator is assessed for the AWGN channel and for the flat fading channels. Simulation results of the MB technique are compared to the limiter-discriminator and the coherent Viterbi detector.

4.1 Performance of the Parametric Frequency Estimators

In this section the performance of the parametric frequency estimators presented in chapter 3 are evaluated for a simple scenario. The signal is composed of a complex sinusoid with normalized frequency f_i equal to 0.5 and additive white Gaussian noise with variance s_w^2.

$$s(n) = A\exp\{j2p(nf_i + j_i)\} + w(n) \qquad (4.1)$$

The length of the data record is N=8 samples, which is a typical value for the over-sampling of GMSK receivers. The SNR is defined here as the ratio of the signal power A^2 to the noise power s_w^2.

The ability of a technique to accurately estimate the instantaneous frequency of the signal is measured by the mean square error [Kay1993]:

$$MSE\left\{\hat{f}_i\right\} = E\left\{\left|f_i - \hat{f}_i\right|^2\right\}, \tag{4.2}$$

where $\hat{f}_i$ is an estimate of the instantaneous frequency f_i. If the estimator is unbiased the mean square error is simply the variance of the estimator.

Provided that the probability density function $p(x,f_i)$ of the quantity to be estimated (the instantaneous frequency in our case) satisfies some regularity conditions [Kay1993], the Cramer-Rao lower bound (CRLB) for an unbiased estimator is defined as:

$$MSE\left\{\hat{f}_i\right\} \geq \frac{1}{E\left\{\left(\frac{\partial \ln p(x, f_i)}{\partial f_i}\right)^2\right\}}. \tag{4.3}$$

The Cramer-Rao bound is a lower bound on the mean square error. Any unbiased estimator will demonstrate a MSE equal to or higher than this bound. For a single sinusoid in AWGN the CRLB for the frequency is [Kay1988]:

$$MSE\left\{\hat{f}_i\right\} \geq \frac{12}{(2p)^2 \times N \times (N^2 - 1) \times SNR}. \tag{4.4}$$

The simulated results of three model-based estimators for a single sinusoid in AWGN (4.1) are presented Figure 4.1 and compared to the CRLB. This figure shows the reciprocal mean square errors of the estimators as functions of the SNR. The results for the discriminator are shown as well. The three model-based estimators are; (1) the covariance method (forward linear prediction) with model order equal to p=3, (2) the modified covariance (forward-backward linear prediction) with p=3 and (3) Kumaresan and Tufts method with a model order of p=6 and only one principal component kept in the decomposition of the autocorrelation matrix. For these three methods, the poles of the parametric filter $\{1,-c_1,...,-c_p\}$ are obtained by rooting, and the angle of the pole with amplitude closest to the unit circle is chosen as the frequency estimate. The frequency estimate for the discriminator is obtain by derivation of the signal phase, summation of the N-1 phase differences and scaling:

$$\hat{f}_{disc} = \frac{1}{2p\,(N-1)} \sum_{n=1}^{N-1} phase\left\{s(n+1)s^*(n)\right\}. \tag{4.5}$$

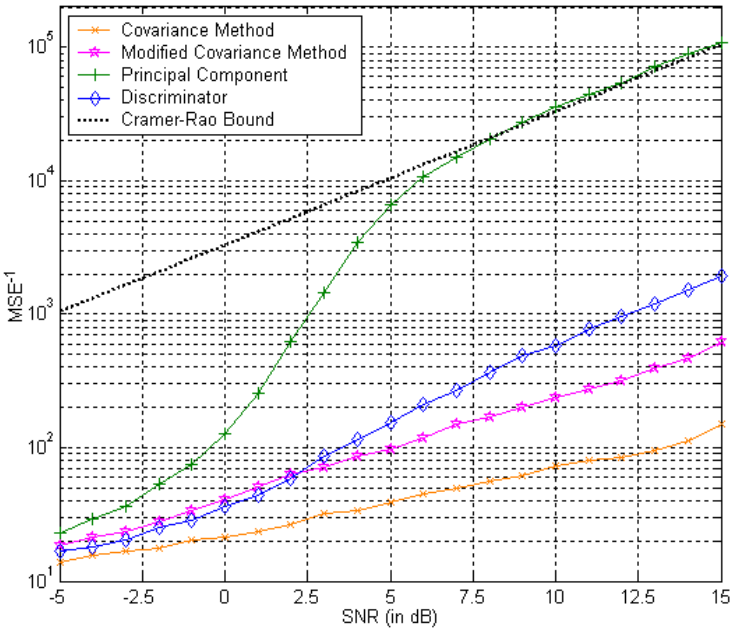

Figure 4.1 Mean square errors of the covariance, modified covariance, principal component methods and discriminator for a single sinusoid in AWGN.

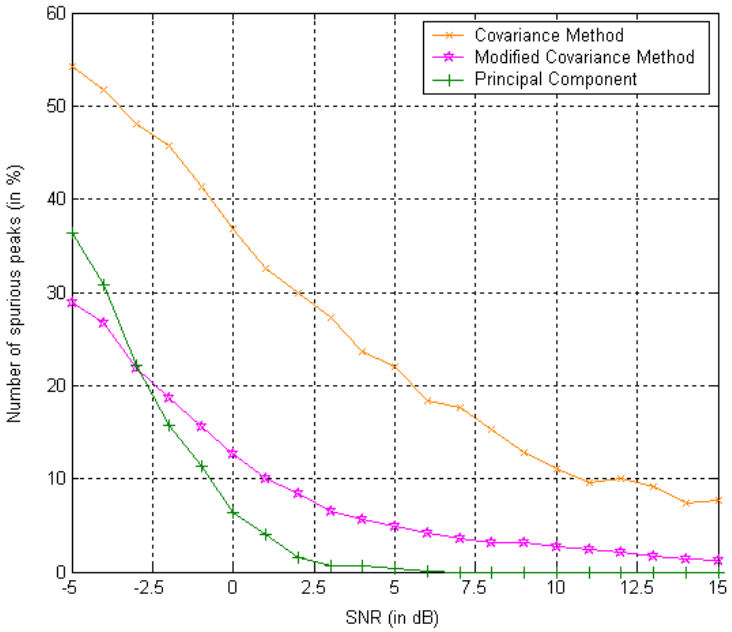

Figure 4.2 Probability of occurrence of a spurious estimation (the pole closest to the true frequency is not selected as the signal pole)

From Figure 4.1, the principal component (PC) technique is seen to be superior to the three other estimators. The PC method achieves the CRLB at around 7 dB, whereas other techniques have inferior MSE performance. As explained in Chapter 3, the difference in performance of the PC technique as compared to the covariance and modified covariance techniques results from the implementation in Kumaresan and Tufts method of noise reduction by subspace decomposition. The direct effect of noise reduction is a decrease in the probability of a spurious estimation (when a noise pole has amplitude greater than the signal pole). A spurious estimation is identified when the pole with largest amplitude is not the pole with angle closest to the true frequency of the sinusoid. Figure 4.2 presents the number of noise poles misinterpreted as signal poles in percentage of the total number of estimations for the covariance, modified covariance and PC techniques as a function of the SNR.

Figure 4.1 clearly demonstrates the superiority of the principal component techniques over the covariance, modified covariance methods and the discriminator when estimating the frequency of a signal similar to (4.1). Further evaluations of those estimators may be found in [Kum1982a], [Wel1996] and [Kay1988]. In particular, simulation results for two sinusoids with frequency spacing of $1/(2N)$ in AWGN are presented in these papers. The performance of the frequency estimators in presence of interference is discussed in more detail in the following section and in the next chapter.

4.2 Adaptation of the Model-Based IF Estimator for MSK Detection

Mean square error curves illustrate the performance of the different techniques as frequency estimators; but those results are insufficient to judge the efficacy of the estimator for use as a demodulator. Since the frequency tones of MSK baseband signal have opposite values, the most straightforward way to use an estimator to detect MSK signals consists in evaluating the frequency of the baseband signal over the bit duration (using the N available samples) and then, generating the bit decision by comparing the frequency estimate to zero. The general block diagram of a model-based demodulator for MSK signals is shown Figure 4.3.

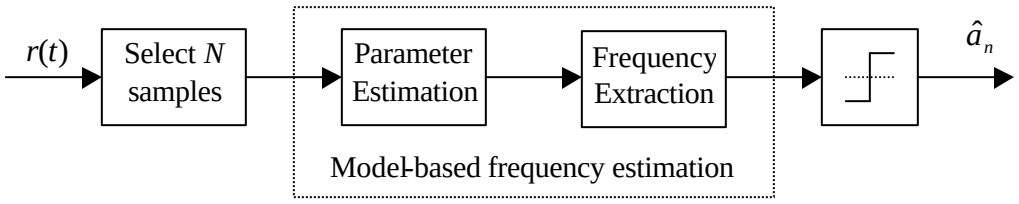

Figure 4.3 Block diagram of a simple model-based demodulator

Whereas a good frequency estimator has low mean square error and performance close to the CRLB, a good detector must correctly estimate the sign of the frequency for most of the trials. The performance of the demodulators is therefore expressed in terms of bit error rate (BER), which is the ratio of the correctly detected bits over the total number of transmitted bits. In the following, the BER performance has been obtained by Monte-Carlo simulations.

The complex MSK baseband signal corrupted by additive Gaussian noise is sampled with an over-sampling factor of N=8 samples per bit. The n^{th} sample of the k^{th} bit can be expressed as:

$$s_k(n) = \sqrt{\frac{E_b}{N}} \exp\{ j2p\,(na_k f_d + j_k)\} + w(n). \qquad (4.6)$$

The complex noise process has variance $s_w^{\,2} = N_O$, and the signal to noise ratio is now defined as E_b/N_O and expressed in decibels. As the model-based detection techniques are non-coherent, the initial phase j_k is assumed to be random with a uniform distribution, and is constant over the bit duration.

Because of the distinct natures of estimation and detection, there is no one-to-one correspondence between the MSE performance of a frequency estimation technique and the bit error rate of the corresponding demodulator. Actually, an inaccurate frequency estimate will result in a bit-error only if it significantly differs from the true frequency. For example, a biased estimator may not necessarily be a bad estimator for demodulation as long as its bias is much less than the frequency deviation and the probability of large error is low. Moreover, depending on the form of the techniques, noise at the output of the frequency estimators may have different probability distributions, so that identical mean square errors for two different techniques may not result in identical bit error rates

for the two corresponding demodulators.

Simulation results for demodulation of an MSK signal corrupted by noise, using the principal component method and the discriminator detector are shown Figure 4.4.a. The principal component method with model order $p=6$, and polynomial rooting (as described in section 4.1) is referred to as the principal component method PC1. At a BER of 10^{-3}, the model-based technique is superior to discriminator detection by about 2 dB.

The performance of various detectors is also assessed in presence of co-channel interference. The behavior of model-based frequency estimators in presence of an interfering signal has been investigated in [Kum1982a], [Wel1996] and [Kay1988]. In addition to being robust to an interfering signal with lower power, the principal component method is also shown in these papers to be capable of estimating the frequency of a signal having equal [Kay1988] and even lower power than the interferer [Wel1996], provided that the relative position of the two frequency tones is known, and that the frequency spacing is sufficient. However, in the case of co-channel MSK signals, the signal of interest (SOI) and the signal not of interest (SNOI) both take frequency $+f_d$ or $-f_d$ with equal probability 0.5. As a result, although the two dominant frequencies of two equal power MSK signals may be estimated it is impossible to associate a particular signal with its corresponding frequency, since a frequency tone will be equally likely to correspond to the first or second MSK signal.

At this point two synchronous co-channel users are considered, the user with strongest power corresponding to the signal of interest. Since the users are synchronous, their frequencies are constant over one bit. From equation 4.6 the expression for the received signal can be written as:

$$s(n) = \sqrt{\frac{E_{b,1}}{N}} \exp\{ j2p\,(na_1 f_d + j_1)\} + \sqrt{\frac{E_{b,2}}{N}} \exp\{ j2p\,(na_2 f_d + j_2)\} + w(n), \qquad (4.7)$$

where both phases j_1 and j_2 have uniform distributions. The signal to interference ratio (SIR) is defined as the ratio of the energies $E_{b,1}/E_{b,2}$ and expressed in dB, $E_{b,1}$ being the bit energy of the signal of interest. The SNR is defined as the value of $E_{b,1}/N_O$ for the stronger signal.

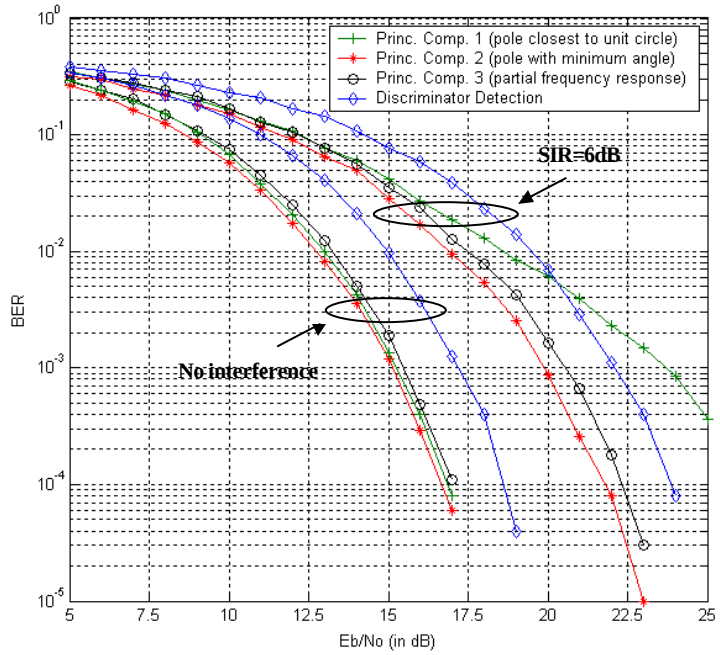

(a)

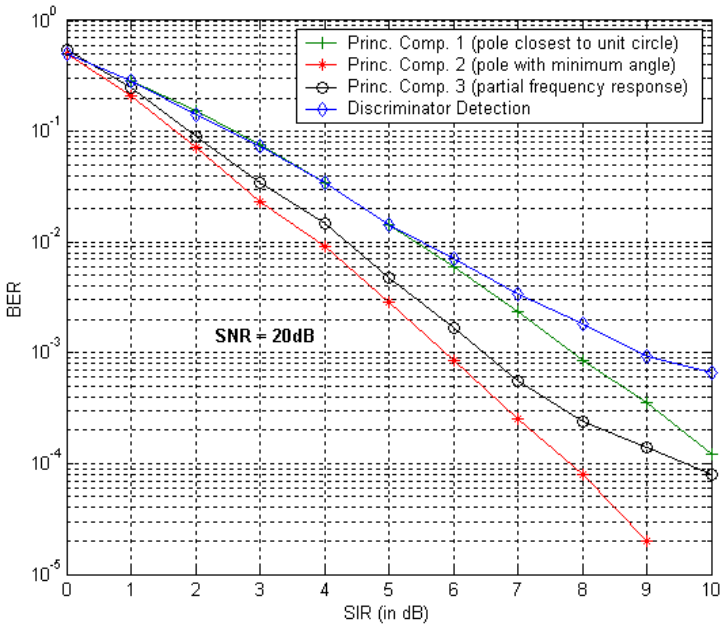

(b)

Figure 4.4 Bit error performance (a) as a function of the SNR and (b) as a function of the SIR of PC detection, with three alternative techniques for extracting the frequency from the model parameters, along with the discriminator.

The detectors are tested for a fixed SIR of 6 dB with SNR varying from 0 to 25dB (Figure 4.4.a), as well as for a fixed SNR of 20 dB with SIR varying from 0 to 10 dB (Figure 4.4.b). For a fixed SIR, the principal component technique (PC1) outperforms the discriminator only for low values of the SNR, and for a fixed SNR, the principal component technique is superior for large values of SIR. Therefore, PC1 is more interference-limited than the discriminator.

So far, the signal pole has been selected as the pole closest to the unity circle, as obtained by the Kumaresan and Tufts method. However, MSK signals have specific characteristics that may be used to improve the frequency extraction from the model-parameters. When choosing the pole closest to the unit circle, the model-based technique may output an estimate that is unlikely to be the frequency of an MSK signal. It is known a priori that the frequency of the baseband MSK signal should be either $+f_d$ or $-f_d$. This frequency deviation f_d is known and equals $f_s/(4N)$, where f_s is the sampling rate. Thus a frequency estimate with large deviation from zero is most probably due to the effect of noise. Therefore it maybe beneficial to choose the pole with angle closest to zero as the signal pole, rather than the pole closest to the unit circle.

Note that the rooting process to obtain the poles from the parametric filter of length $p+1$ has complexity $O(p^3)$ (the roots of the polynomial are found by eigenvalue decomposition of the companion matrix). Alternatively, estimation of the magnitude of the filter response for K values of frequency only requires $O(pK)$ operations. Since demodulation of the MSK signal does not necessitate precise estimation of the signal frequency (only the sign of the estimate is of importance), by appropriately choosing the set of frequencies tested, a partial frequency response of the filter may be sufficient to correctly decide on the transmitted bit. In the same way since the pole with closest angle can be chosen after rooting, a-priori information about the signal can be used to reduce the probability of error; the only frequencies for which the filter response needs to be tested are frequencies that lie between the two MSK tones. This restriction on the frequency range tested also helps reduce the complexity of the spectrum estimate. Finally, the estimate is chosen as the frequency with peak response within the partial spectrum.

The performance of three different implementations of the principal component

method (results for PC1 having already been discussed above) are seen on Figure 4.4.a and Figure 4.4.b. Estimation of the model parameters is identical for the three model-based techniques and employs Tufts and Kumaresan method. The order of the model is $p=6$, and only the first component of the SVD is selected to approximate the autocorrelation matrix. Extraction of the instantaneous frequency from the estimated parameters is performed using three alternative techniques summarized below, as well as using the standard discriminator.

1- *PC1*: The poles of the parametric filter are obtained by rooting. The pole closest to the unit circle is chosen as the signal pole and its angle gives an estimate for the frequency.

2- *PC2*: Similarly to method 1, the poles of the parametric filter are obtained by rooting. However, the signal pole is chosen as the pole with smallest angle.

3- *PC3*: The frequency response of the parametric filter is estimated for 16 frequencies, uniformly distributed between $+f_d$ and $-f_d$. The frequency corresponding to the maximum magnitude is selected as the estimate.

4- *Discriminator detection*: The frequency estimate is obtained by discrimination of the signal phase and integration over the bit duration.

As observed from these figures, the use of a-priori information in method PC2 and PC3 leads to superior performance as compared to the blind model-based technique PC1. With this improvement, the principal component techniques outperform the discriminator in both noise and interference limited environments. Also, the principal component technique with reduced complexity, using the partial filter response to estimate the peak frequency (PC3), has worse performance than the polynomial rooting technique (PC2) by only 0.5dB. In the following, the principal component technique is used with polynomial rooting and selection of the root having minimum frequency deviation (PC2), which is seen here to have the best performance among the three proposed schemes. However, PC3 technique should not be disregarded, as it allows some adjustment between the complexity and the performance; this technique has a lower complexity when the filter response is measured for a few frequencies, while it can potentially achieve performance equal to the polynomial rooting technique when the spectrum is estimated for a large number of values.

4.3 Sequence Estimation with Model-Based Detection

4.3.1 Pre-Detection Filtering and Sequence Estimation

Prior to detection, the narrowband received signal is converted to a lower frequency (intermediate frequency or IF) and then filtered to remove the high frequency components and obtain the baseband complex envelope of the signal. When it has narrow bandwidth, the IF filter also alters the complex envelop of the signal and this effect is simulated by incorporating a pre-detection filter into the block diagram of the baseband receiver. For a MSK matched filter receiver, this pre-detection filter degrades the performance, as the baseband signal after filtering does not exactly correspond to the matched filter. However, in some cases a narrow bandwidth for the IF filter is used on purpose, in order to improve the performance of the detection. While the pre-detection filter introduces inter-symbol interference, which should degrade the performance, it also reduces the noise power at the input to the detector. By appropriately choosing the filter, such that the signal to noise power is maximized while the ISI is kept at a reasonable level, performance of the detector may be greatly improved. Optimization of the pre-detection filter for conventional receivers has been intensively studied, as it has a major impact on the overall performance of the system. The effect of pre-detection filtering is now investigated in the specific case of model-based detection.

The use of a filter to help reducing the observation noise at the input of a parametric frequency estimator is one of the possible methods proposed in [Kay1988] to obtain more accurate frequency estimates. The validity of this approach is confirmed by the fact that the maximum likelihood frequency estimator itself involves some implicit filtering. The pre-detection filters used in the simulations are Gaussian. Figure 4.5 shows the impulse response of the Gaussian filters for different values of the time bandwidth product ($B_{IF}T$).

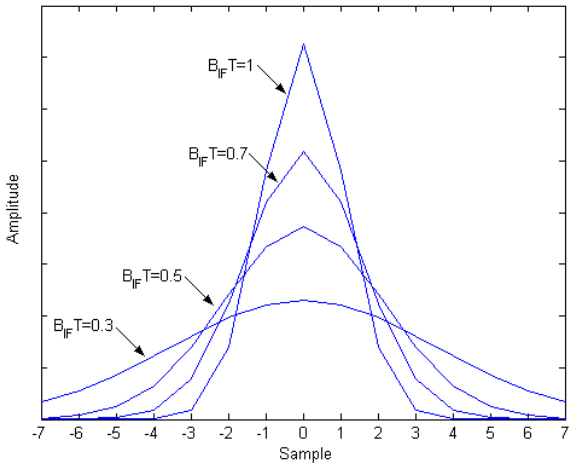

Figure 4.5 Digital Gaussian filters for a sampling rate of N=8 and $B_{IF}T$ varying from 0.3 to 1

The pre-detection filter increases the inter-symbol interference. For large values of the filter bandwidth, the filter is almost zero outside $[-T/2;T/2]$ and the memory introduced by the filter is T, whereas for small values, like $B_{IF}T$ = 0.3, the filter is non-zero over $[-T;T]$ and the memory introduced by the filter is 2T. Unless specified, all of the IF filters are truncated to $[-T;T]$ in our simulations.

After filtering, the frequency of the received signal is estimated using the principal component method (PC2). Due to the presence of inter-symbol interference, the frequency estimate not only depends on the value of the current symbol but also on the surrounding symbols. For a noise free channel with total memory length L (the channel length is here the sum of the lengths of the modulation pulse-shape and pre-detection filters) the maximum number of possible values for the frequency estimate is 2^L. As the Gaussian pulses are symmetrical, the number of distinct points is usually slightly less. Therefore a trellis of 2^{L-1} states followed by the Viterbi algorithm can be used to track the frequency. For a given symbol n, the distance metric from state i to state j is the Euclidian distance between the ideal (noiseless) frequency estimates $f_n(i \to j)$ and the measured value $\hat{f}_n$:

$$v_n(i \to j) = \left(\hat{f}_n - f_n(i \to j)\right)^2 \qquad (4.8)$$

For each state two transitions are allowed, corresponding to the transmission of ‘0’ or ‘1’.

The branch metric is set to infinity if the transition between states i and j is not allowed. The Viterbi algorithm returns the sequence of symbols with maximum likelihood, assuming that the frequency estimate is corrupted by Gaussian noise. Although this assumption is inexact (the distribution of noise at the output of the estimator is not Gaussian), sequence estimation employing the Viterbi algorithm is still nearly optimum. Also, the use of a sequence estimation scheme after the frequency estimator is possible only since the signal phase is continuous: if the phase was discontinuous between consecutive symbols, the ISI at the output of the frequency estimator would also depend on the relative phases of the consecutive symbols.

4.3.2 Multiple Frequency Estimates per Symbol

For the previously described model-based demodulators, the frequency of the signal was estimated once every bit over the N available samples for this bit. For MSK signals without filtering, the estimate obtained only depends on the value of the current symbol. The set of samples selected for estimation may be seen as a sliding window of size $L_W = N$, sliding by steps of $S_W = N$ samples between two consecutive estimates. When the frequency is estimated using a set of L_W samples in between two consecutive symbols, the frequency estimate depends on the value of the two adjacent bits.

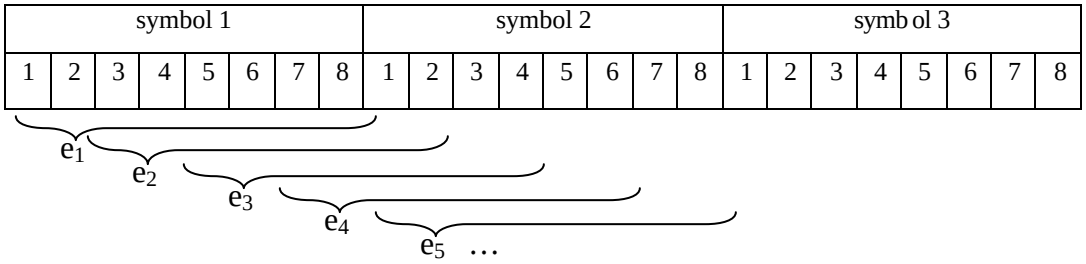

Figure 4.6 Example of a sliding window for the model-based estimator (L_W = 8, S_W = 2)

Figure 4.6 shows a sliding window of size $L_W = 8$ samples with hops of $S_W = 2$ samples between two consecutive estimates. The resulting number of estimates per bit is equal to $N/S_W = 4$. The output of the estimator may be filtered and dumped to obtain one averaged frequency estimate per bit, or alternatively, all the estimates may be used to track the frequency of the signal. In the example shown Figure 4.6, the estimations e_2, e_3

and e_4 have intermediate values between e_1 and e_5. While the estimation of these intermediary values requires additional computations, it provides extra information to the sequence estimation process.

There are now N/S_W estimates between two consecutive symbols, and the track of the frequency between these two symbols employs approximately 2*N* samples. In the previous example, starting from e_1, the frequency estimates up to the next symbol are e_2, e_3, e_4 and e_5; and the estimation of these frequencies employs almost all of the samples composing symbols 1 and 2. Thus, the number of possible frequency paths is now doubled and equals 2^{L+1}, where L is the channel length. These frequency paths may be plotted to form an eye diagram as in Figure 4.7. The possible values for the frequency estimates are shown for a receiver that employ a Gaussian pre-detection filter with $B_{IF}T$=0.3 and length L_{IF}=2 for respectively (a) MSK signals and (b) GMSK signals.

In Figure 4.7.a, the channel has length L=3. At time 0, there are 6 ($<2^L$) possible values for the frequency estimate. These values correspond to the scenario $L_W = N$ and $S_W = N$ (one estimate per bit), which was considered in the beginning. When using the intermediate values of the frequency (values between times t=0 and T), the total number of paths is $16=2^{L+1}$. Figure 4.7.b shows the eye diagram at the output of the model based (MB) frequency estimator when the signal is GMSK, that is an ISI of length L=5. The total number of paths in the eye pattern is therefore 64.

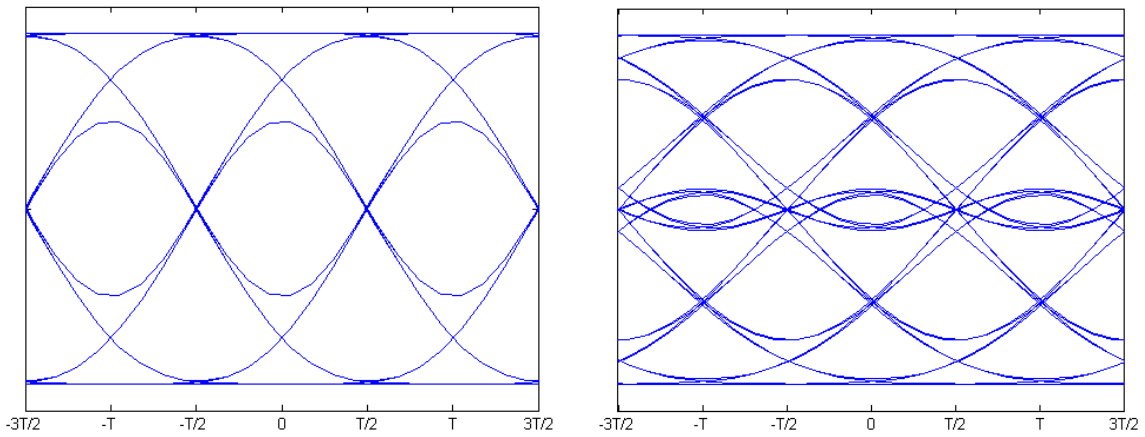

(a) (b)

Figure 4.7 Eye pattern of the model-based frequency estimator output for (a) MSK and (b) GMSK signals. The pre-detection filter is Gaussian with $B_{IF}T$ = 0.3.

The possible frequency transitions are then represented by a trellis diagram. Each state of the trellis corresponds to a possible sequence of L bits: the number of states required in the trellis is equal to half the number of paths in the eye pattern, as two transitions are possible for each state of the trellis. The track of the frequency in the trellis is accomplished employing the Viterbi algorithm.

With N/S_W estimates per bit (EPB), the branch metric for an allowed transition is the sum of N/S_W terms:

$$v_n(i \to j) = \sum_{k=1}^{N/S_W} \left(\hat{f}_n(k) - f_n(k, i \to j) \right)^2 . \qquad (4.9)$$

where $\left\{ \hat{f}_n(1), ..., \hat{f}_n(N/S_W) \right\}$ is the set of the N/S_W frequency estimates for the current symbol, and $\left\{ f_n(1, i \to j), ..., f_n(N/S_W, i \to j) \right\}$ is the theoretical path for the frequency (noiseless estimates) corresponding to the transition of state i to state j. The general block diagram of the model-based demodulation employing pre-detection filtering and sequence estimation is presented Figure 4.8.

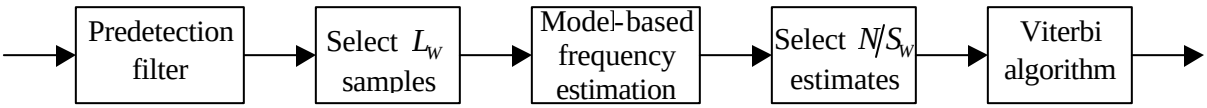

Figure 4.8 Block diagram of a model-based sequence estimator

4.3.3 Performance of Model Based Sequence Estimation Schemes

The diverse implementations proposed in the previous section for the MB demodulation of MSK signals are simulated and their performance is compared for the Gaussian channel. The parametric frequency estimation is identical for all schemes and was referred to as the PC2 method in part 4.2; it employs the Kumaresan and Tufts technique with a model order of $¾ N = 6$ and the first principal component of the SVD. The frequency is extracted from the pole of the parametric filter having angle closest to zero. Five distinct demodulation schemes are implemented with and without IF filtering,

symbol level detection or sequence estimation, and single or multiple estimates per bit (EPB). The legend of cases considered is as follows:

1- *Simple MB detection (PC2)*: the frequency is estimated once per bit using the N=8 samples available ($L_W = 8$, $S_W = 8$). The bit is decided according to the sign of the frequency estimate.

2- *Symbol-level decision, 1 EPB*: the signal is filtered prior to the detection. Then the frequency estimation and the detection are identical to case 1.

3- *Symbol-level decision, 8 EPB*: the received signal is filtered, and then its frequency is estimated 8 times every bit ($L_W = 8$, $S_W = 1$). The output of the frequency estimator is filtered, dumped and compared to zero.

4- *Sequence estimation, 1 EPB*: the received signal is filtered, its frequency is estimated once a bit ($L_W = 8$, $S_W = 8$). The soft output of the estimator is utilized to compute the decision metrics of an 8 state trellis.

5- *Sequence estimation, 8 EPB*: the frequency of the filtered signal is estimated 8 times per bit ($L_W = 8$, $S_W = 1$). The frequency is then tracked using the Viterbi algorithm and a 16 state trellis.

The simulated performance of the five-demodulation schemes above is presented Figure 4.9. The pre-detection Gaussian filter implemented for the symbol-level demodulation schemes (methods 2 and 3) has time-bandwidth product equal to $B_{IF}T$=0.5, while the sequence estimation schemes (methods 4 and 5) make use of a filter with $B_{IF}T$=0.3. The major performance improvement over the simple detection (method 1), results from the implementation of the pre-detection filter. For a bit error rate (BER) of 10^{-3} the required SNR of method 2 is reduced by 4dB as compared to the first method. Then the use of sequence estimation gives an additional 2dB improvement of the model-based technique (method 4). Utilization of multiple estimates per bit does not improve the performance of the symbol-level detection schemes: method 3 has performance inferior to method 2. However, when combined with sequence estimation (method 5), the use of the intermediate frequency estimates further reduces the performance by 1dB at a BER of 10^{-3} as compared to method 4.

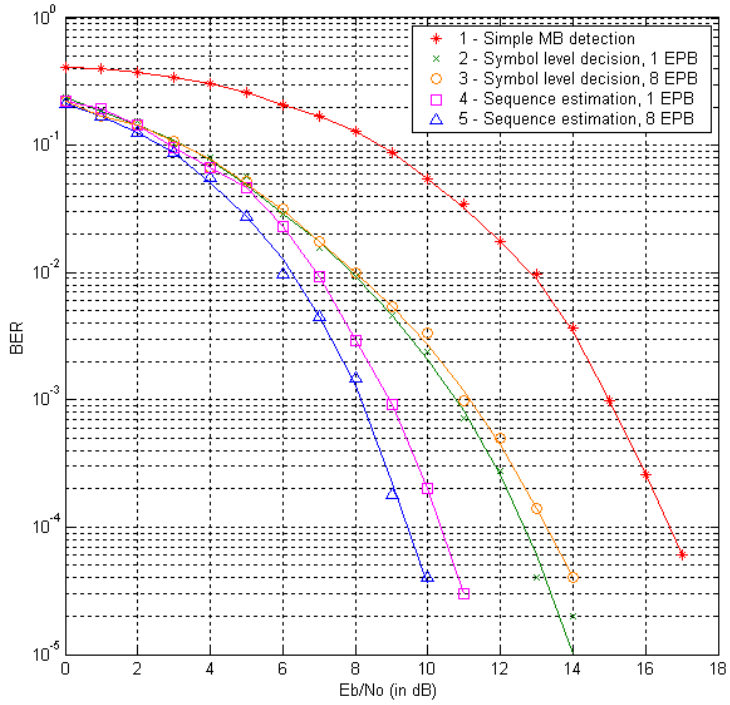

Figure 4.9 Simulation results in AWGN of five model-based demodulators for MSK, with (1) no pre-detection filter, and (2,3,4,5) Gaussian pre-detection filter; (1,2,4) single and (3,5) multiple frequency estimations per bit; (1,2,3) symbol-level detection and (4,5) sequence estimation.

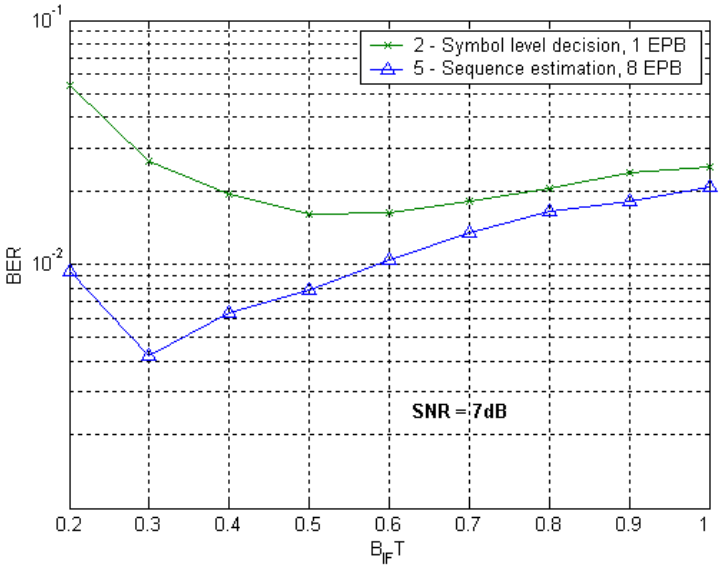

Figure 4.10 Performance of (2) the MB symbol detection, and (5) MB sequence estimation at SNR=7dB as a function of $B_{IF}T$.

The effect on the performance of the bandwidth of the pre-detection filter for the symbol-level MB decision with 1 EPB (method 2) and MB sequence estimation with 8 EPB (method 5) is presented Figure 4.10. For all values of $B_{IF}T$ the sequence estimation technique outperforms the symbol-level decision. However, the best performance for method 2 and 5 are obtained for different values of $B_{IF}T$. $B_{IF}T$=0.5 is optimum for method 2 whereas $B_{IF}T$=0.3 is optimum for the MB sequence estimation. These values for $B_{IF}T$ have been employed previously (Figure 4.9).

4.4 Performance of the MB Demodulation with AWGN and Flat Fading

Two channels are considered in this section: the Gaussian channel and the quasi-static channel with Rayleigh fading. The performance of the model-based sequence estimation technique (MB) is compared to the coherent Viterbi detector (VD) and a sequence estimation scheme with limiter-discriminator detection (LD). Also the simulation results are shown for MSK and GMSK (BT=0.25) signals.

The Viterbi detector is simply composed of a bank of four filters matched to MSK signals followed by a Viterbi processor. This demodulator is MLSE for MSK in the Gaussian channel. The limiter-discriminator scheme (see Figure 2.10) is composed of a pre-detection filter, a discriminator and a Viterbi detector. The model-based demodulator uses the sequence estimation technique presented in the previous section (method 5). In order to allow a fair comparison, the pre-detection filters for the model-based demodulator and the discriminator are identical. Also, all sequence estimators implemented in this section for the non-coherent schemes are based on 16 state trellises.

The first set of simulation results (Figures 4.12.a and 4.12.b) presents the performance of the three demodulation-techniques in AWGN. The pre-detection filter used in Figure 4.12.a for the non-coherent schemes is a Gaussian filter with $B_{IF}T = 0.5$. For Figure 4.12.b, the pre-detection filter is Gaussian with $B_{IF}T = 0.3$; which is the optimum value for the sequence estimation schemes with model-based (Figure 4.10) and discriminator detection and MSK signaling.

Figure 4.11 shows the number of states required in the sequence estimation process to mitigate the effect of all interfering symbols. A trellis with a number of states

lower than indicated in this table would not take all interfering symbols into account and would have reduced performance, whereas a trellis with more states than this value can give optimum results but has needless complexity. A number of states equal to 16 is therefore sufficient for all proposed implementations of the discriminator and of the model-based detector, except for the case of GMSK (BT = 0.25) with pre-detection filter of length 2T and model-based estimation.

Length of the Predetection Filter	L_{IF} = *1*		L_{IF} = 2	
Modulation Format	MSK	GMSK	MSK	GMSK
Total Channel Length	L = 2	L = 4	L = 3	L = 5
LD	2 states	8 states	4 states	16 states
MB (8 EPB)	4 states	16 states	8 states	32 states

Figure 4.11 Number of states required in the post-detection trellises after LD and MB detection for MSK and GMSK signals and pre-detection filters with length L_{IF}=T and 2T

It is seen in Figure 4.12.a and Figure 4.12.b that the MLSE technique is superior to non-coherent techniques in AWGN for demodulation of MSK signals. Also, the degradation of the performance for GMSK signals with the MSK optimum detector is only 0.6 dB at a bit error rate of 10^{-3}, as compared to MSK. The Viterbi detector has the best performance for demodulation of GMSK signals. Among the non-coherent schemes, the model-based technique outperforms the discriminator in all four cases (MSK and GMSK, $B_{IF}T = 0.5$ and $B_{IF}T = 0.3$). While the simple MB scheme had performance superior to the simple discriminator by about 2 dB (Figure 4.4.a), the improved MB sequence estimation scheme has performance superior to LD sequence estimation by only 1 dB. Moreover, the improvement of MB technique for GMSK demodulation is less for $B_{IF}T = 0.3$ than for $B_{IF}T = 0.5$, which possibly results from the non-optimum size of the trellis employed after the MB detection (a trellis of 32 states would be optimum for GMSK signaling).

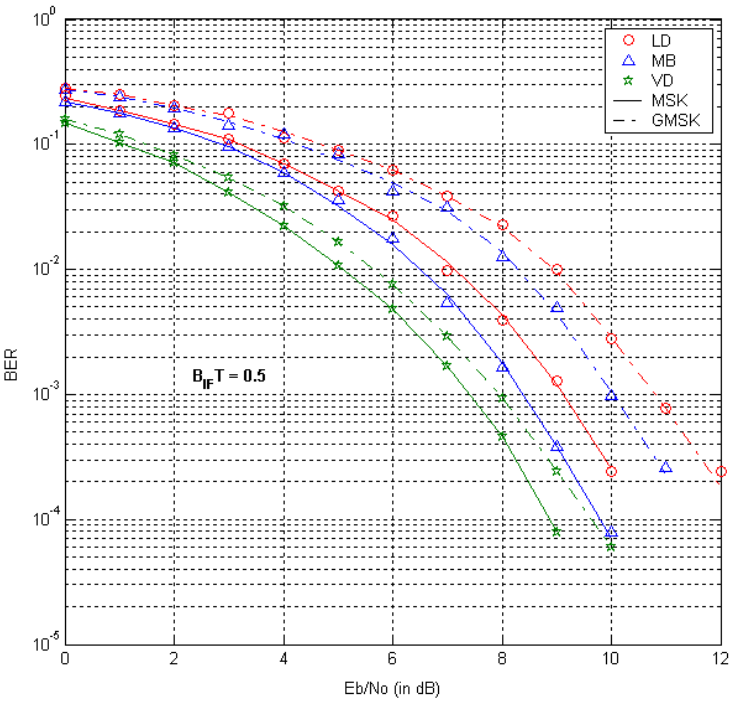

(a)

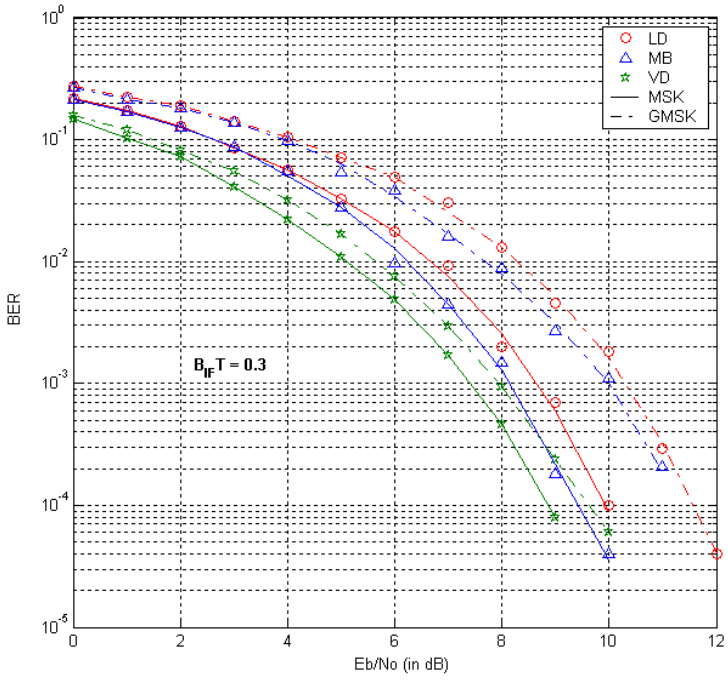

(b)

Figure 4.12 Simulated performance in AWGN of the LD, MB and VD techniques, for MSK and GMSK signals. Results for the LD and MB methods are shown when (a) $B_{IF}T$ equals 0.5 and (b) 0.3.

While the behavior of the demodulation schemes in the Gaussian channel is fundamental, the mobile channel is also subject to fading. Fading is caused by the superposition at the receiver of multi-path components of the transmitted signal. Each path contributes to the received signal with a different time delay, which results from diverse scattering of the transmitted signal; this effect is called flat fading. At the receiver, the different components add in a constructive or destructive manner, depending on their relative phases. The overall result of flat fading is a change in the amplitude of the received signal, by some factor, called a fading coefficient.

In general, the fading coefficient is time varying and random. To be able to simulate the effect of flat fading, a common assumption is that the fading coefficients follow a Rayleigh distribution [Rap1996]. Also, in practical mobile channels with reasonably large transmission rates, it has been observed that the time coherence of the fading channel is usually larger than the frame durations; in other words, the fading coefficient changes slowly as compared to the transmission rate. Therefore, over a short period of time, the channel may be assumed to be invariant.

In the simulation, the value of the fading coefficient is chosen to be constant over a sequence of 100 bits and this coefficient is Rayleigh distributed. Also, there is no time correlation between the fading coefficients of successive sequences. This corresponds to a quasi-static channel. The performance of MB, LD and VD techniques with slow flat fading are shown for MSK signals (Figure 4.13.a) and for GMSK signals (Figure 4.13.b). In both cases, the time-bandwidth product used for the pre-detection filters of MB and LD schemes is $B_{IF}T = 0.3$. It is seen in these figures that similarly to the case of the Gaussian channel, the performance of the MB techniques with slow flat fading lays in-between VD and LD detection. For a target BER of 10^{-3}, there is about 2 dB of difference between the performance obtained for MSK and GSMK signals.

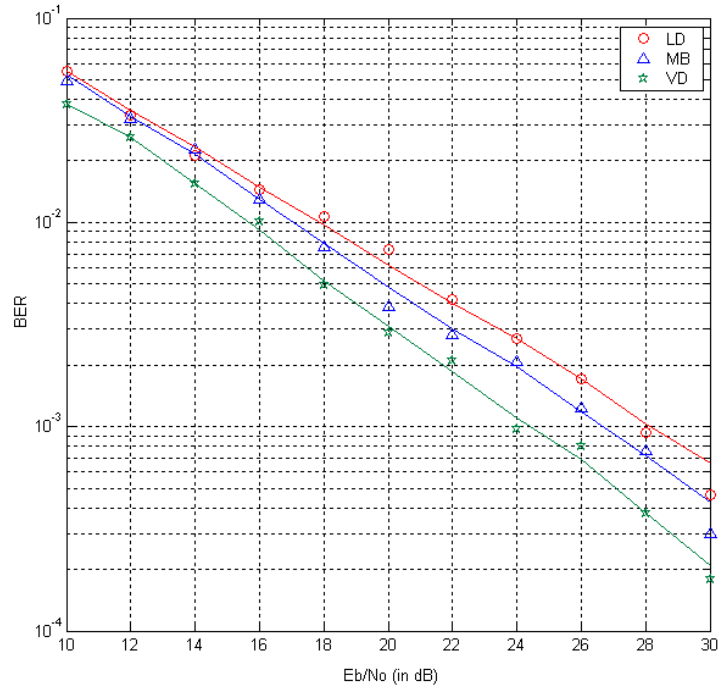

(a)

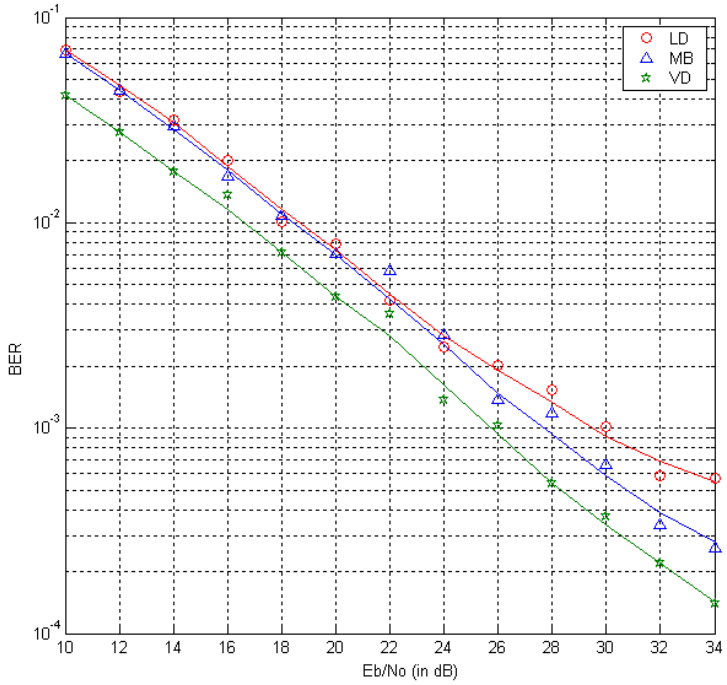

(b)

Figure 4.13 Performance with slow flat fading of LD, MB and VD techniques for (a) MSK signals and (b) GMSK signals.

4.5 Summary

In this chapter, we implemented the Kumaresan and Tufts parametric frequency estimator for the demodulation of MSK and GMSK signals. This principal component technique, with minor modifications, permits the detection of MSK signals with low error rates for medium SNRs. To be able to detect the signal in poor channel conditions, the MB demodulation is combined with pre-detection filtering and sequence estimation (Viterbi algorithm). These two techniques respectively reduce the input noise and mitigate inter-symbol interference. An increase in the number of frequency estimates per bit is also shown to improve the performance of sequence estimation schemes with model-based detection.

Finally, the performance of the model-based technique is assessed through computer simulations in two channel conditions: with AWGN and slow flat fading. The advanced MB scheme is shown to be superior to discriminator detection and have performance approaching coherent detection in the Gaussian and flat fading channels. However, the resistance of MSK demodulation techniques to co-channel interference has not been considered yet. This resistance to CCI is of prime importance as it determines the capacity of narrowband cellular systems and is investigated in Chapter 5.

Chapter 5 Interference Rejection Capability of Model-Based Demodulation

A model-based demodulator for MSK and GMSK signals has been described in Chapter 4, and the simulation results for this demodulator were obtained for the AWGN and slow flat fading channels. The interference rejection capability of the base-station receiver is a major concern in mobile systems. The model-based demodulator is now assessed in the presence of co-channel interference (the only modulation format considered is MSK) and its performance is compared to some other demodulation schemes. In addition, demodulator diversity is introduced as a way to improve the CCI rejection capability of individual receivers, and a combined scheme is proposed for demodulation of MSK in CCI limited environments.

5.1 Performance of Standard Techniques with CCI

The capacity of a cellular system in a noise-limited environment can be increased by reducing the size of the cells until the interference between the co-channel users (CCI) of adjacent cells becomes the dominant impairment. Therefore, the ability of the base-station receivers to reject CCI will determine the minimum size for the cells and greatly impact on the overall system capacity.

The closed-form analysis of co-channel interference is not easy, since the probability distribution of the interfering signals is complex. In [Chi1996] the performance of GSMK and BPSK in presence of co-channel interference is considered. Whereas a closed-form expression is derived for BPSK, results for GMSK are obtained by simulation only. In some cases the effect of CCI may be modeled as AWGN. For instance, the distribution of a single co-channel interferer in a generic angular modulation system is shown in [Cho1999] to be Gaussian in slow Rayleigh fading. The Central Limit Theorem implies that the sum of several CCI (with independent fading) and thermal noise, all of these processes having Gaussian distribution, will be Gaussian. Therefore, with the appropriate correspondence between CCI and the equivalent amount of Gaussian noise, performance of CPM schemes with CCI and slow Rayleigh fading can be

approximated by the results in AWGN.

However, in general, the Gaussian hypothesis is only applicable when the number of interferers is very large. When only a few interferers are present, the performance may significantly differ from the Gaussian approximation. In [Chi1996] the Gaussian approximation is seen to overestimate the bit error rate for BPSK and GMSK signals with CCI. Also, in a small-cell cellular environment, co-channel interference is likely to originate from a few signals. Adaptive antenna techniques as well as smart channel assignment both contribute to reduce the number of co-channel interferers [Chi1996]. For these reasons, the robustness of these demodulation techniques for a single CCI is primarily investigated in this chapter.

The performance of the conventional demodulator for GMSK in presence of co-channel interference has been simulated in [Yao1996], [Ada1990], [Lop1991]. In [Yao1996] different implementations of the differential detector are compared. It is seen that decision feedback equalization helps mitigate the interference. A 2-bit differential detector (DD) with 2-bit decision feedback (DF) outperforms 1-bit and 2-bit DD without DFE and 2-bit DD with 1-bit DF. Limiter-discriminator schemes are considered in [Ada1990] with various post-detection techniques. The MLSE post-detection scheme offers superior performance than DFE in a co-channel interference-limited environment. Simulations results in [Ada1990] are double-checked with field experiment. Finally, a comparison of non-coherent and coherent demodulation for GMSK in CCI is performed in [Lop1991]. While coherent and non-coherent schemes offer very different results in AWGN, limiter-discriminator and coherent detection have closer performance to a single CCI [Lop1991]. In section 5.4 the performance of the model-based demodulator for MSK and GMSK demodulation in presence of CCI is compared via computer simulations to some of these standard techniques.

5.2 Co-channel Interference Rejection Techniques for MSK Signals

Various co-channel interference rejection techniques are possible in narrowband systems; such as time division multiple access and frequency hoping (which is also narrowband over short periods of time). In this section some multiuser detection and interference cancellation techniques are overviewed. Some other methods for CCI

rejection are presented in [Las1997b]. The multiuser detection and interference cancellation techniques have been intensively studied in the context of code division multiple access [Ver1998]. But the extension of the multiuser detection techniques to the narrowband GMSK signals is not straightforward, as GMSK modulation is non-linear and non-antipodal. Moreover, depending on the phase and misalignment of the signals, the matched filters for the co-channel users may have a very similar form, which makes two equal power GMSK signals difficult to separate.

The optimum demodulator for the co-channel signals is the joint maximum sequence estimation technique (JMLSE). For a single user and pulse duration of LT, the optimum Viterbi detector for a unique MSK signals has 2^{L+1} states. In presence of a co-channel user, each state of the first user can be matched with one of the 2^{L+1} state for the second user. As a result the optimum detector has $(2^{L+1})^2$ states [Mur1995]; in [Ran1995] a JMLSE receiver employing a 256 states trellis is simulated. The resulting complexity makes the use of optimum joint detection impractical.

As seen in chapter 2, the MSK format can be represented as a special case of OQPSK with sinusoidal pulse shaping. It is shown in [Lau1986] that GMSK signals can also be represented as a finite sum of pulse amplitude modulated (PAM) signals; this is called the Laurent representation. Based on this representation new receivers have been developed for GMSK signals. Approximation of GMSK signals with the principal components of the Laurent decomposition has lead to reduced complexity single-user receivers. Also, in [Mur1996], this representation has been employed to build optimum and sub-optimum joint detectors. Finally, the PAM representation by Laurent facilitates the analytical analysis of GMSK.

The optimum joint detectors for MSK-type signals employ the Viterbi algorithm with large trellises. Alternatively, the sub-optimum decision driven multiuser detectors can offer good resistance to co-channel interference with reduced complexity [Ver1998]. Among the decision-driven detectors, successive interference cancellation has been investigated in [Ars2000] and [Ars2001] for narrowband signals. The output of the single-user receiver is used to reconstruct the strong signal; this reconstructed signal is then subtracted to the observed signal and the demodulation of the difference gives an estimate for the weak signal. Therefore, successive interference cancellation permits the

demodulation of the weak signal. Also, by reconstructing and subtracting the weak signal to the original signal, the estimate of the strong signal may be improved.

Another joint detector for FM signals is presented in [Ham2000]. For a complex signal composed of two constant envelop sinusoids with known amplitudes, the instantaneous phase of each sinusoids (two unknowns) may be calculated from the real and imaginary parts of the sum. However, there is an ambiguity in the calculation and two sets of phases are possible at each instant, one of which corresponding to the true values. The algorithm proposed in [Ham2000] tracks the possible phases and selects the values that minimize the instantaneous frequency. This approach can be applied to demodulate CPFSK signals. However, as the effect of noise is neglected in this technique, this non-coherent joint detector has good performance for high SNR only.

For successive interference cancellation and for other joint detection techniques as well, an accurate estimation of the amplitude and phase for all co-channel users is required. The estimation of these parameters necessitates complex channel estimation processes, employing per survivor processing (PSP) for example, and introduces additional losses.

5.3 Simulation Results of the MB Demodulator in CCI limited Environment

5.3.1 Degradation of the Performance in Presence of CCI

In this section, the performance of the model-based demodulators is simulated in presence of co-channel interference. The co-channel interferers are either synchronous to the signal of interest (the bit periods of the SOI and SNOI are time-aligned at the receiver) or asynchronous. In presence of M equal-power interferers, the signal to interference ratio (SIR) is defined as $E_{b,S}$ / ($M\times$ $E_{b,I}$), and expressed in decibel. For M=1 the SIR is simply the ratio of the signal power, $E_{b,S}$, to the interferer power, $E_{b,I}$. Also, the signal to noise ratio is measured relatively to the signal of interest.

First, the performance of four model-based schemes among the one proposed in section 4.3.c is simulated in presence of a unique asynchronous interferer. These techniques respectively employ symbol-level detection with 1 EPB, symbol-level detection with 8 EPB, sequence estimation with 1 EPB, and sequence estimation with 8 EPB and were referred to as methods 2, 3, 4 and 5 in section 4.3.c.

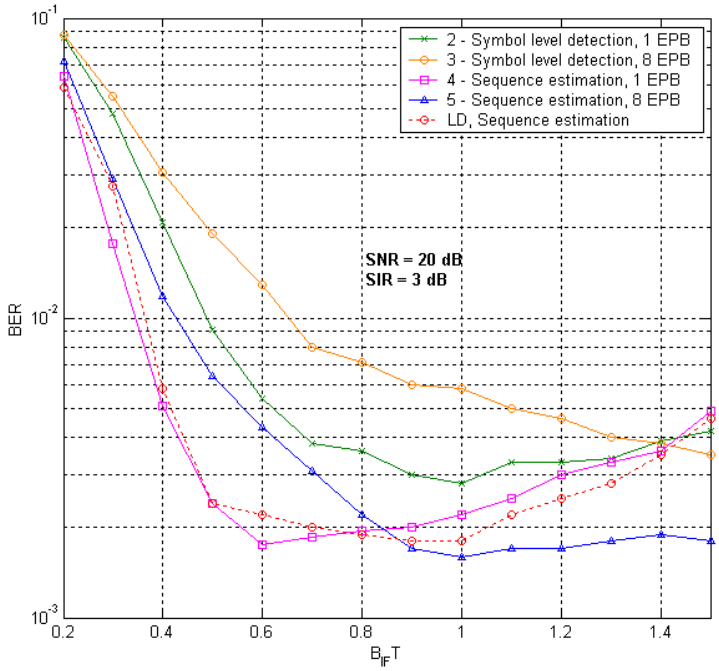

Figure 5.1 BER versus IF filter bandwidth for MSK, with MB demodulation (methods 2, 3, 4 and 5) and limiter-discriminator detection.

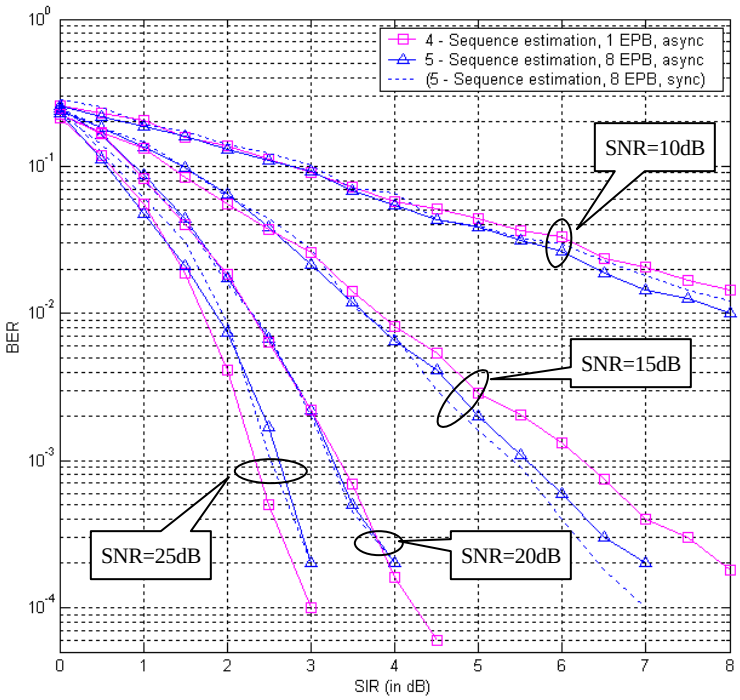

Figure 5.2 Simulated BER of MB sequence estimation, with 1 EPB (method 4, $B_{IF}T = 0.6$) and 8 EPB (method 5, $B_{IF}T = 1$). The results are shown in presence of a synchronous and asynchronous (method 5 only) interferer. E_b/N_O =10, 15, 20, 25 dB.

The BER is seen Figure 5.1 as a function of the IF filter bandwidth, $B_{IF}T$, with a SNR of 20dB and a SIR equal to 3dB. The simulation results obtained for the sequence estimation scheme with discriminator detection are shown as well. It is seen that, in the Gaussian channel, the choice of the IF filter greatly impacts the overall performance of the demodulation. Similarly, in presence of CCI, different values for the IF filter leads to different performance. Method 4 achieves his minimum error rate for $B_{IF}T = 0.6$, whereas $B_{IF}T = 1$ is the optimum value for method 5. Regardless of this dependence on $B_{IF}T$, the performance for the MB sequence estimation schemes (4,5) is superior to that for the MB symbol-level detection (2,3).

The error probabilities of the two model-based sequence estimation schemes are compared as functions of the SIR and with E_b/N_O =10, 15, 20, 25 dB (Figure 5.2). The time-bandwidth products for method 4 and method 5 are respectively chosen to be 0.6 and 1, which are seen Figure 5.1 to be the optimum values for these techniques (at SNR=20dB and SIR=3dB). The difference in performance for the two schemes in these various CCI conditions is less than 0.5 dB for most cases. Due to its better resistance to noise, method 5 has slightly superior performance for low SNR, whereas the other technique (method 4) employing 1 EPB is more robust to CCI when the SNR is large. Although the complexity of method 4 is significantly less than method 5, the MB results presented later in this chapter are derived for method 5 exclusively. Also, as observed in Figure 5.2, the BER for method 5 when the interfering user is synchronous is close to the asynchronous case.

The effect of multiple interfering signals is now investigated. The number of interferers is $M = 1, 2, 3, 10, \infty$; the interferers are all asynchronous and equal-power. Thus, for a fixed SIR, the power of each interferer depends on M, such that the total interference power is constant. For an infinite number of interferers, the Gaussian approximation applies (central limit theorem); the effect of AWGN and CCI is simulated as a unique Gaussian process having power equal to the sum of the noise power and the total interference power. The simulated BER probability of method 5 in presence of multiple interferers is reported Figure 5.3. The signal to interference ratio is equal to 6 and 10 dB.

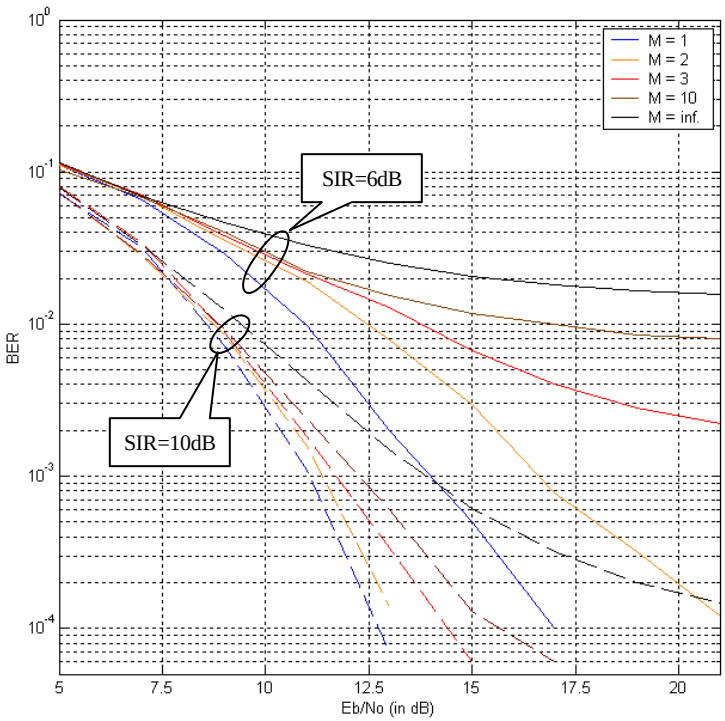

Figure 5.3 Bit-error probability versus SNR for MSK with MB demodulation and $M = 1,2,3,10,\infty$ interferers and SIR=6,10dB

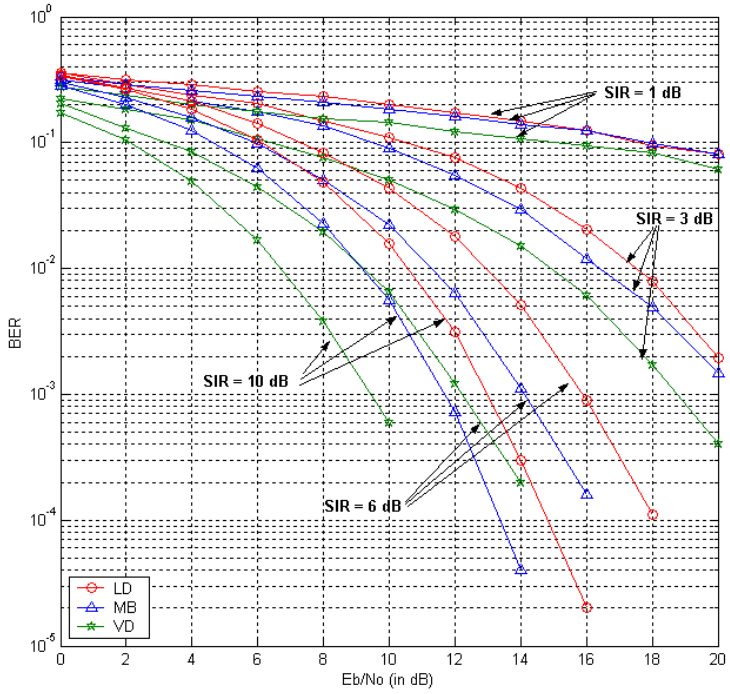

Figure 5.4 Performance comparison of LD, MB and VD techniques with one interferer; SIR=1,3,6,10dB

As obvious from Figure 5.3, there is a large difference between the single and multiple interferer cases. With the increasing number of interferers, the performance of the MB demodulator decreases until the special case of $M = \infty$, where the distribution of the interferers becomes Gaussian. These results confirm the fact that the Gaussian approximation ($M = \infty$) is only valid for a large number of interferers [Chi1996].

5.3.2 Performance Comparison of LD, VD and MB Demodulation

From Figure 5.2, the optimum value for the time-bandwidth product before discriminator detection with sequence estimation is $B_{IF}T = 1$, similarly to the model-based method 5. The results for MB (method 5, $B_{IF}T = 1$), LD ($B_{IF}T = 1$) and VD demodulation techniques are plotted Figure 5.4, in presence of a unique asynchronous interferer and with SIR=1,3,6,10dB. Again, the coherent Viterbi detection outperforms the two other schemes (as in the AWGN case). Also, the MB demodulator ranks first among the two non-coherent sequence estimation techniques. For a targeted BER of 10^{-3}, and with SIR=6dB, there are 2dB of difference between the required SNR of the MB and Viterbi detectors and an additional 2dB of difference between the MB and LD techniques. All three techniques have limited performance for low SIR even for large values of the SNR; and for negative SIR (the SOI is the weak signal), the SNOI would be demodulated instead of the SOI.

The distinction of the SOI and SNOI is only possible if there exist some difference between the signals. There are four parameters that differentiate two MSK co-channel interferers: the phase, the delay, the instantaneous frequency and the amplitude. For the non-coherent frequency estimation techniques such as the MB or LD demodulators, the signals are mainly distinguished based on their instantaneous frequency and amplitude (the strong user is demodulated). However, when the interfering signals have almost equal power, the estimation of the frequency of the received signal is not sufficient to distinguish the two users, since two strictly co-channel signals may have identical instantaneous frequencies, depending on their transmitted bits. The presence of a shift between the carrier frequencies of the two users could help in differentiating the signals.

5.3.3 Effect of a Doppler Frequency Offset

The shift of the carrier frequency of the received signal resulting from the relative displacement of the transmitter and the receiver is well known as the Doppler effect. For a relative velocity of n_d between the two elements, the frequency shift of the carrier is:

$$f_d = n_d / l \ , \tag{5.1}$$

with l denoting the wavelength of the signal. In cellular systems, the base station has a fixed position whereas the handset may move at speed as high as a car on a highway. For a wavelength of the order of the GHz, the maximum Doppler shift is typically around 100Hz (corresponding to a carrier frequency of 900MHz and a relative speed of 75 mph). In the airborne scenario however, the base-station may be a high-speed aircraft and the resulting Doppler frequency can be of the order of 500Hz (with the same frequency band this corresponds to a relative speed of around $160\ \text{m.s}^{-1}$ or 310 knots). Whereas the Doppler spread of the signal limits the transmission rates of conventional receivers, it also introduces some dissimilarity between the co-channel users, which may be exploited to recognize the user of interest.

The parametric frequency estimators are able to correctly separate distinct sinusoids with frequencies as close as $f_S/(2N) = R/2$ [Wel1996], where f_S is the sampling rate and *R* is the bit rate. Also, MSK tones have frequency equal to $f_d = \pm R/4$. Therefore, two MSK signals with carrier frequencies respectively equal to f_{c1} and f_{c2} cannot be completely separated unless $|f_{c2} - f_{c1}| > R$. When the difference between the carriers is greater, the parametric spectral estimator outputs two distinct poles for the two signals, while when the difference is less there may be only one pole representing the two signals.

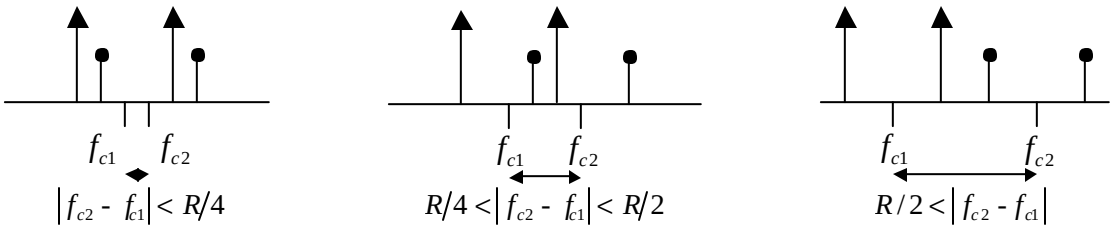

Figure 5.5 Relative positions of the frequency tones for two MSK signals with carrier frequencies f_{c1} and f_{c2}: three alternative scenarios.

However, a user with carrier frequency spaced by more than R from the signal of interest is unlikely to be a co-channel user. For two co-channel signals, the carrier frequencies at the transmitter are identical. The received signals however may have different frequencies due to different Doppler shifts but this frequency deviation is limited. For a bit rate of $R = 10$ kbps for instance, and if the difference in frequency of the two carriers, due to the Doppler effect, is 1kHz, then, $|f_{c2} - f_{c1}| = R/10$. Such a large Doppler spread is unlikely to happen and is still less than the minimum frequency difference required for the parametric estimator to output two distinct poles for the SOI and the SNOI.

The bit error rates of the model-based technique, the discriminator and the Viterbi detector are evaluated in presence of one SNOI having frequency slightly offset from the frequency of the SOI (Figure 5.6). The frequency difference $|f_{c2} - f_{c1}|$ ranges from 0 to $R/2$, the SNR is 20 dB, and the SIR is 3dB. For the MB and LD detections, the simulation results are shown for an IF time-bandwidth product of $BT_{IF} = 1$. Also, the exact frequency of the signal of interest is assumed to be known by the receiver.

According to this figure, not only does a frequency shift of the interferer not help the detection of the SOI, but it even degrades the performance. The BER increases with the increase in the frequency shift, until $|f_{c2} - f_{c1}| = R/4$. For the large frequency shifts the performance is improved, since the predetection filter attenuates the interference. Also, as anticipated from Figure 5.4, the LD and MB techniques have similar performance for $|f_{c2} - f_{c1}| = 0$. However, with the increasing difference between the carrier frequencies, the performance of the MB technique becomes superior to that of the discriminator. Although the range of frequency differences considered in Figure 5.6 may not be typical for a Doppler shift, this result suggests that the robustness of MB detection to random FM interference is improved as compared to LD technique.

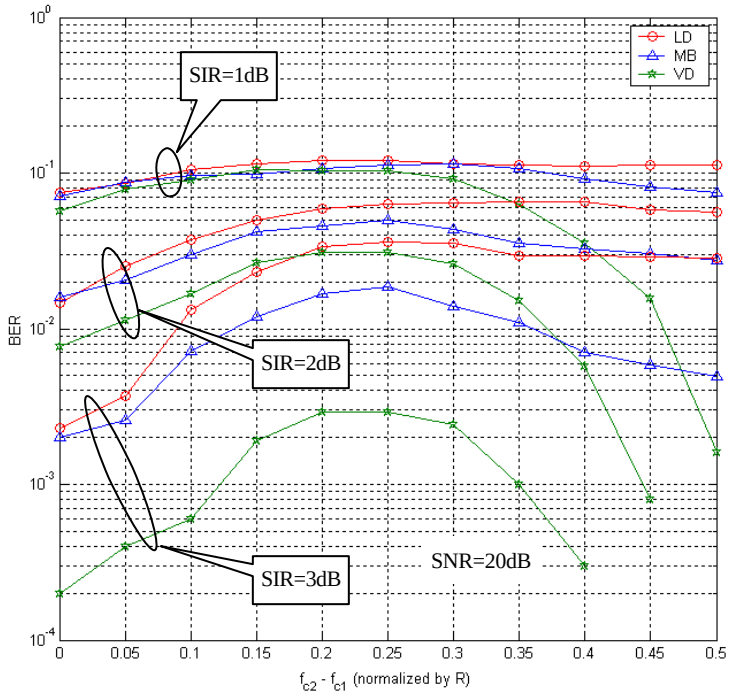

Figure 5.6 BER versus frequency offset of the interferer for LD, MB and VD demodulation techniques, SNR=20dB, SIR=1,2,3dB

5.4 Demodulator Diversity: a Combined MB / VD Scheme

5.4.1 Demodulator Diversity

There does not exist a single best demodulation scheme for GMSK: for each channel a different demodulators may be optimum. For that reason, one has to carefully estimate the wireless channel of interest before selecting an appropriate demodulation scheme. Rather than choosing a single technique, which may not be the best in all scenarios, attempts have been made to use several techniques at the same time and use this demodulation diversity to obtain the best possible performance. For instance, a smart receiver employing a bank of *K* demodulators could select the output of a given demodulator depending on the channel (demodulator 1 for AWGN channel, demodulator 2 in CCI limited environment, demodulator 3 in slow fading…). However, due to the possible superposition of all these effects a simple selection of one demodulation technique is not satisfactory. Instead, the soft-output of the *K* demodulators can be weighted and added together as shown on Figure 5.7 (the signals $r_1,r_2,\ldots,r_K$ are identically equal to the received signal).

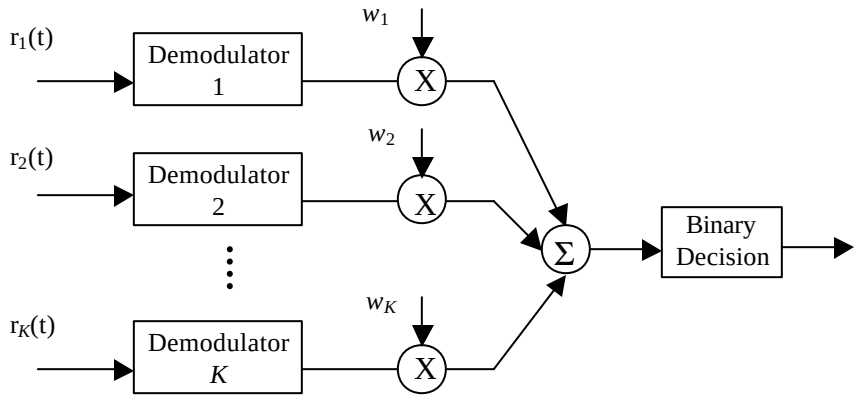

Figure 5.7 Block diagram of a post detection combiner

Such post-detection combiners have been developed in the case of antenna diversity. To combat fading, a receiver may comprise several antennas, with large spacing to limit the correlation of the fading profiles at each antenna. The set of the *K* signals $r_1,r_2,\ldots,r_K$ (received from the different antennas) may be co-phased and added before detection, but this pre-detection combining requires the tracking of the signal

phase for each antenna. Post-detection combining, on the other hand, may be used with non-coherent detection [Ada1988b]: the individual signals from each antenna are demodulated independently and the K soft outputs are then combined before decision. The possible methods for combining the soft outputs are equal gain combining, maximum ratio combining and adaptive combining.

5.4.2 A Combined Demodulator for MSK

Demodulator diversity for GMSK signals is investigated in [Las1997a]. The author chooses to combine several coherent and non-coherent demodulators. It is then shown in this paper that the adaptive combined scheme has performance at least equal to the best demodulator in all channel conditions and that in some cases (with CCI and urban fading) the combined scheme may even outperform the best individual scheme. In this part, a combined demodulation scheme for MSK signals is proposed, employing MB and VD techniques.

The combination of the model-based and the coherent techniques to improve the performance was suggested by the comparison of the outputs of the MB demodulator and of the Viterbi detector. While the probability of a bit error is less for the Viterbi detection than for the MB demodulator in the Gaussian channel and in presence of an interferer (Figure 5.9), only a few of these bit errors are common for the two techniques. It is seen in Figure 5.9 that the probability that the MB and VD techniques simultaneously make an error for the same bit is much less than the probability of bit error of each individual schemes. In other words, if there existed a genie that would be able to select the output of the demodulator that gives the correct decision, this genie would have performance equal to the probability of common errors (when both demodulator outputs are incorrect even the genie is fooled). Obviously, such a genie does not exist. However, there exist some measures for the correctness of the bit decision: one of them is the distance metric in the trellis diagrams. As both MB and VD demodulation techniques employ a trellis to track the signal (or its frequency as in the case of MB method), the decision metrics of the two diagrams may be combined to improve on the individual decision. For instance, due to the combination of noise and interference, the Viterbi detector may decide a sequence of bits that is incorrect. This sequence has the lowest metric in the VD trellis. However, on

the MB side, the same sequence of bit may correspond to a very large metric in the MB trellis, telling that this sequence is not correct.

The combined MB/VD demodulation scheme, which has been implemented, is based on a coherent Viterbi detector (4 state trellis) and a model-based sequence estimation technique with 8 frequency estimations per bit. The IF filter preceding the model-based detection is Gaussian, has large bandwidth ($B_{IF}T = 1$) and its time duration is truncated to one bit. The model-based technique itself would therefore employ a 4 state trellis for the sequence estimation process (Figure 4.11). Then a trellis is built such that each state (i_{VD}) of the VD trellis is combined with each state of the MB trellis (i_{MB}). There are a total of 4×4=16 possible states (i_{VD}, i_{MB}) in the combined trellis. For a valid transition, the decision metric from state (i_{VD}, i_{MB}) to state (j_{VD}, j_{MB}) is the sum of the individual decision metrics, weighted by a factor $m_{MB/VD}$:

$$u_{MB/VD,n}\left((i_{VD}, i_{MB}) \to (j_{VD}, j_{MB})\right) = m_{MB/VD} \times u_{VD,n}(i_{VD} \to j_{VD}) + u_{MB,n}(i_{MB} \to j_{MB}), \quad (5.1)$$

where the decision metrics $u_{VD,n}(i_{VD} \to j_{VD})$ and $u_{MB,n}(i_{MB} \to j_{MB})$ have been defined in Equations 2.11 and 4.9 respectively. A valid transition is a transition $\left((i_{VD}, i_{MB}) \to (j_{VD}, j_{MB})\right)$ such that both transitions $(i_{VD} \to j_{VD})$ and $(i_{MB} \to j_{MB})$ are allowed and lead to an identical bit decision. The decision metric is set to infinity if the transition is not allowed.

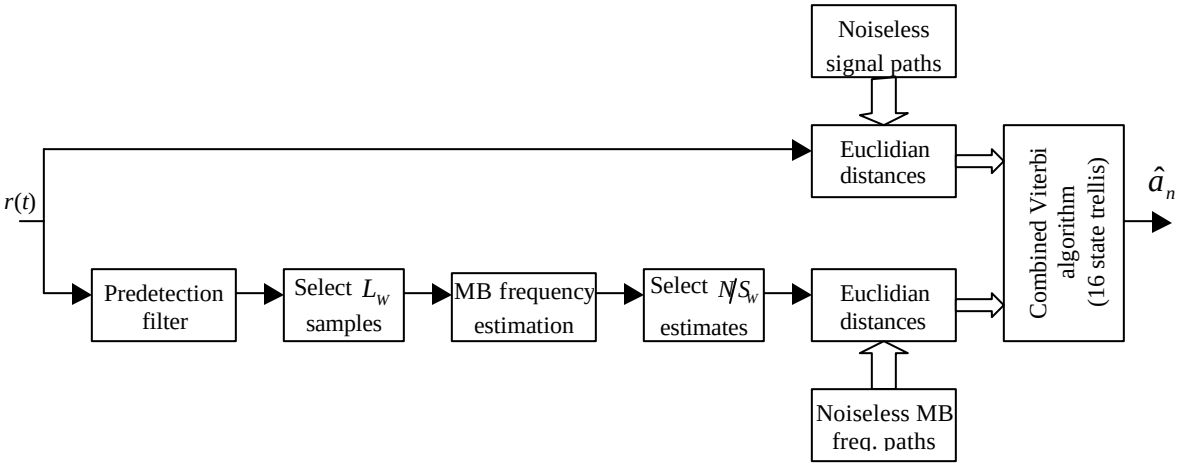

Figure 5.8 Block diagram of the baseband combined MB/VD demodulator

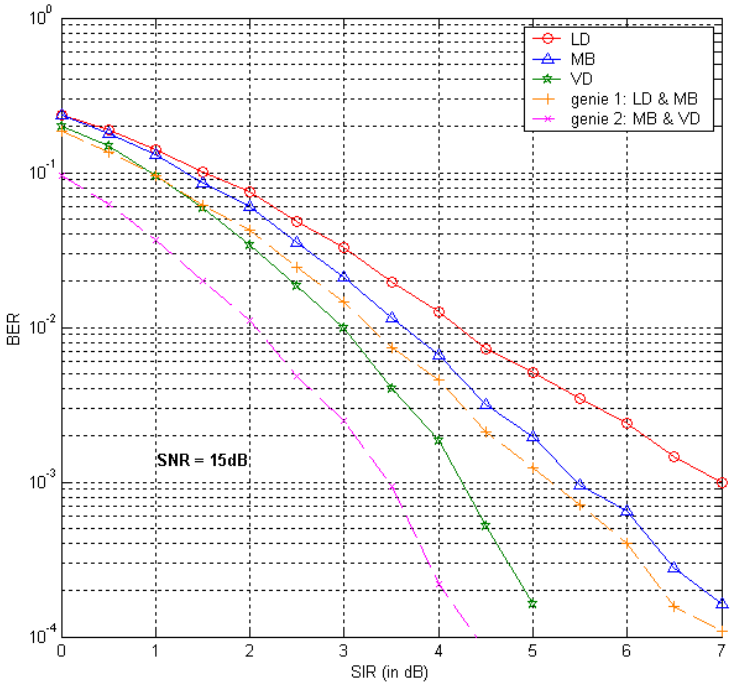

Figure 5.9 Common errors between LD and MB techniques (genie 1), and between MB and VD techniques (genie 2) in presence of CCI and with SNR=15dB, along with the performance of the individual schemes.

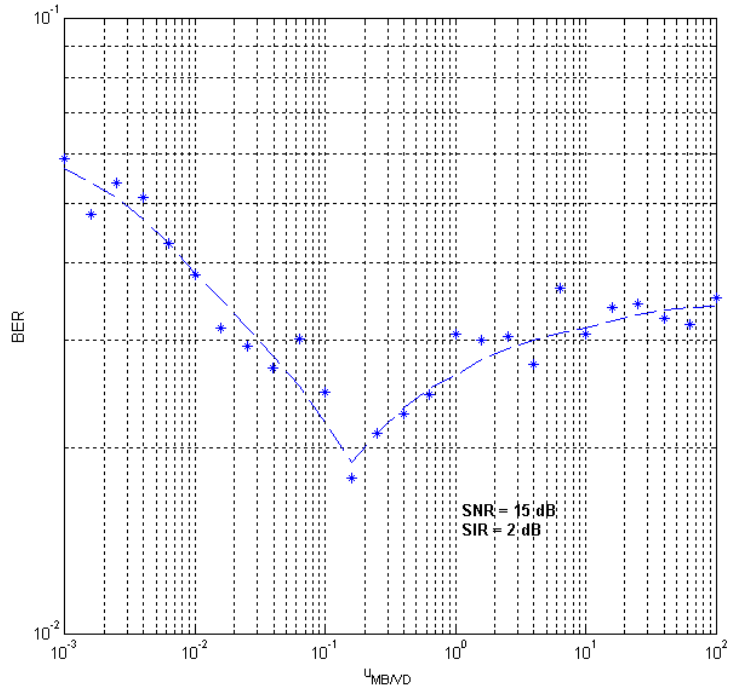

Figure 5.10 BER versus m_{MBVD} for the combined MB/VD scheme with SNR=15dB and in presence of a co-channel interferer; SIR=2dB

The factor $m_{MB/VD}$ is constant and determines the relative contribution of the VD and MB metrics to the decision: for a large value of $m_{MB/VD}$ the performance of the combined scheme approaches that of VD technique, whereas for small values of $m_{MB/VD}$ the combined scheme has results similar to MB sequence estimation. The performance of the combined scheme is shown Figure 5.10 in presence of one interferer (SIR=2dB) and AWGN (SNR=15dB) as a function of $m_{MB/VD}$. As previously explained, for extreme values of the weighting factor, the results for the combined scheme approach those for the individual techniques. However, the BER curve has a minimum between these two extreme scenarios, corresponding to the optimum combination of the decision metrics. The optimum value for $m_{MB/VD}$ depends on the SIR and SNR. When employing maximum ratio combining (MRC) the weights of the decision metrics before combining should be updated for each value of the SIR and SNR. However for simplicity, $m_{MB/VD}$ is fixed to its optimum value at SIR=2dB and SNR=15dB (corresponding to the minimum BER of Figure 5.10); resulting in a small degradation of the performance.

Before presenting the results for the MB/VD schemes, it may be noted from Figure 5.9 that the number of common errors between LD and MB sequence estimation techniques is large. As this probability of common error is a lower bound for the performance of the combined scheme, it has not been tried to implement this combined MB/LD scheme.

The simulation results for the combined MB/VD scheme are shown Figure 5.11 and Figure 5.12. For comparison, the results of the VD and MB demodulators are also reported on these figures. Figure 5.11 presents the result of the combined scheme in AWGN. The MB branch of the combined technique utilizes an IF filter with $B_{IF}T = 1$. For this value of the time-bandwidth product, the performance of MB technique itself is inferior to VD by more than 2dB. The combined scheme however has performance approaching Viterbi detection (there is less than 0.5dB of degradation). The superiority of the VD technique to the MB/VD is expected since the coherent Viterbi detection is the MLSE (optimum) in AWGN. Moreover, the weighting coefficient chosen for MB/VD is optimized for a CCI scenario; the best value for $m_{MB/VD}$ in AWGN would be $m_{MB/VD} = \infty$, such that the MB/VD results match the MLSE performance.

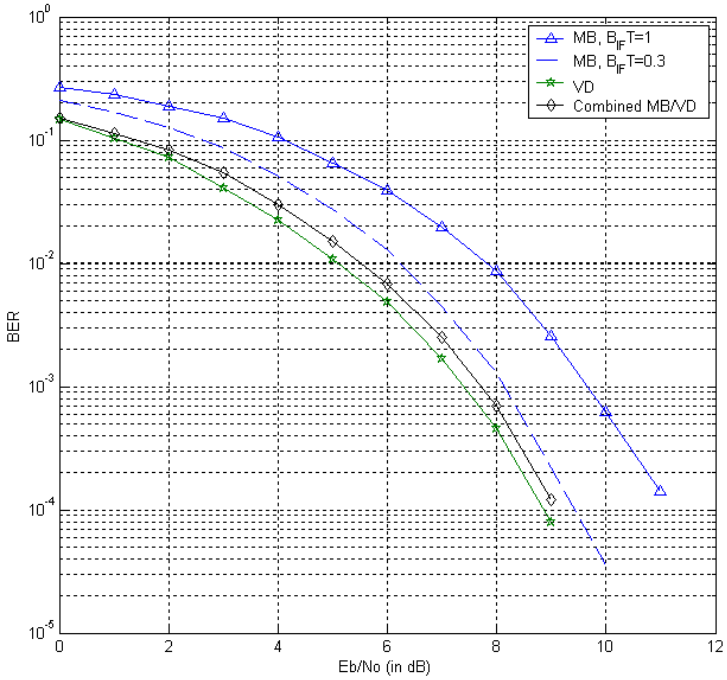

Figure 5.11 Simulated BER versus E_b / N_O for the MB ($B_{IF}T = 1$ and $B_{IF}T = 0.3$), VD and combined MB/VD techniques

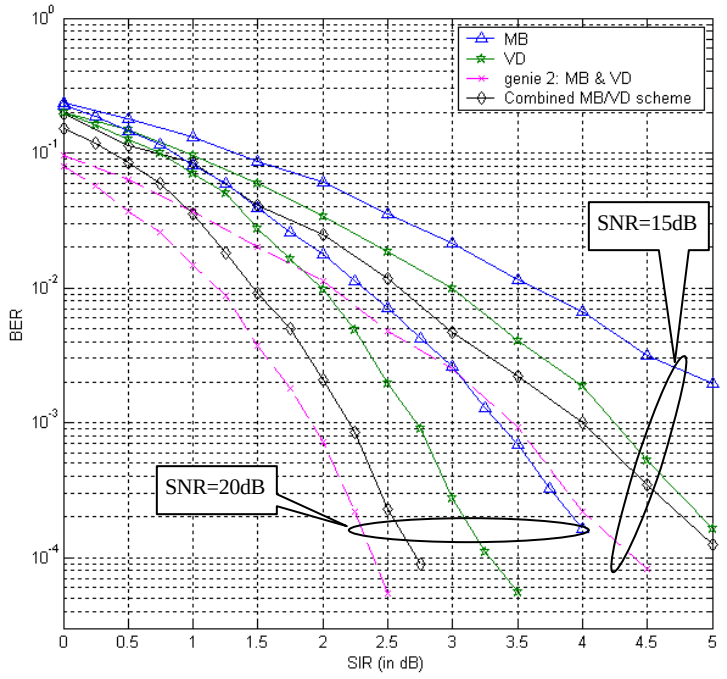

Figure 5.12 Performance of the combined MB/VD scheme in presence of CCI and with SNR=15 and 20 dB along with the results for the MB, VD and genie approaches.

In AWGN the VD technique cannot is superior to any other demodulation scheme. But, in presence of CCI the coherent detector has sub-optimum performance, and therefore a demodulation scheme employing diversity combining may give an improved result as compared to the simple Viterbi detector. Actually, it is seen in Figure 5.12 that the MB/VD demodulator is superior to the VD technique in presence of an asynchronous interferer and with SNR=15 and 20dB. The difference in performance at BER=10^{-3} between the VD and MB/VD schemes is 0.25dB when SNR=15dB and more than 0.5dB when SNR=20dB (in terms of minimum SIR required to achieve the target BER). In determining the dependence of the overall capacity of narrowband systems to the robustness of the receiver to CCI, this small difference may be significant.

Also, a combined MB/VD scheme could be of interest as the first stage of an SIC receiver. Due to the error propagation problem in successive interference cancellation, the performance of the first stage (demodulation of the strong signal) acts as a bottleneck for the following stages of SIC. For two co-channel signals, it has been observed that the probability of bit error for the demodulation of the weak user is similar to the BER for the strong user when the SNR is large. Therefore, a SIC receiver employing the combined MB/VD receiver to demodulate the strong signal (and a simpler receiver at the second stage) could achieve good performance when the difference in power of the two signals is as low as 2dB and the SNR=20dB.

5.5 Summary of the Simulation Results

5.5.1 Advantages of MB Demodulation

The model-based sequence estimation scheme proposed in Chapter 4 has been simulated for MSK signals with co-channel interference. The performance was shown for different SNR and SIR in the case of a single and multiple CCI, the interferers were either synchronous or asynchronous, and the possible shift of the carrier frequency of the interferer was investigated. The simulation results of the MB technique with CCI are slightly superior to the limiter-discriminator, but the coherent receiver outperforms the MB scheme. An improved MB/VD receiver, which exploits demodulation diversity, is presented, with performance surpassing the other simulated schemes.

5.5.2 Complexity of the MB Techniques

The performance comparison of the model-based demodulation with the standard non-coherent receivers, and the comparison of the combined scheme with the conventional coherent receivers have shown the possible benefits of MB techniques. However, the computational complexity of such techniques should not be ignored.

To obtain the model parameters, the principal component technique employs a singular value decomposition (SVD) of the data matrix X. This matrix has dimension $2(N-p)\times p$ for the modified covariance method. For a $M_1 \times M_2$ matrix, with $M_1 \le M_2$ the SVD has a computational complexity of $O(M_1^2 M_2)$ (the number of additions and multiplications are proportional to $M_1^2 M_2$) [Gol1989]. Therefore, the complexity of the SVD for the data matrix X is $O(\{2(N-p)\}^2 p)$ when $p \ge 2N/3$. Then the extraction of the frequency from the estimated parameters requires either the evaluation of the frequency response of the parametric filter for K frequencies which has complexity $O(pK)$, or rooting of the polynomial which is $O(p^3)$. Those operations are necessary for each frequency estimate. When the number of estimate is greater than the number of bits ($S_W < N$), the complexity of the detection is multiplied by N/S_W.

Finally, tracking the frequency using the Viterbi algorithm necessitates further computations: for a trellis of 2^{L+1} states, which is employed in the MB sequence estimation process for a channel of order L-1 and multiple estimates per bits, the computational complexity is $O(2^{L+2})$ [Ver1998]. The computational complexity of the limiter-discriminator with Viterbi equalization and of the coherent Viterbi receiver are principally attributable to the Viterbi algorithm employed in these techniques. On the contrary, for reasonably small trellises, the complexity of the parametric frequency estimation dominates the overall complexity of the MB demodulation.

Chapter 6 Conclusions and Future Work

6.1 Conclusions

In this thesis, parametric frequency estimation and its application to demodulation of CPM in presence of CCI were investigated. In the first part of the thesis (Chapter 2 and Chapter 3), MSK modulation format and parametric frequency estimation were overviewed. In Chapter 2, we detailed the properties of MSK and GMSK signals and the most common demodulation schemes available for these modulation formats. In Chapter 3 we described the modified covariance and the principal component methods to estimate the parameters of the autoregressive model and presented two techniques to extract the frequency from these parameters.

In the second part (Chapters 4 and 5), various demodulators for MSK, employing parametric frequency estimation were proposed. The performance of these schemes was assessed via computer simulations and compared to some of the conventional demodulation techniques. In Chapter 4, a model-based demodulator employing sequence estimation was implemented. For MSK and GMSK signals, in AWGN and flat fading, this technique outperforms discriminator detection and approaches the performance of coherent detection. The behavior of these diverse techniques in presence of interference was investigated in Chapter 5. Additionally, demodulator diversity was proposed as a way to improve the performance of the individual schemes. It was seen that, with CCI, a technique combining model-based and Viterbi detection is superior to the simple coherent Viterbi detector.

The implementation of a non-coherent model-based sequence estimator for MSK signals and the study of demodulation diversity combined with model-based approach, are the two main contributions of this thesis. These proposed model-based receivers have good CCI rejection capabilities, which make them attractive for applications in which CCI is very problematic like the airborne scenario.

The limitations to the model-based approach were also investigated in Chapter 5. In particular, the computational complexity is a major drawback of parametric frequency

estimation. Also, autoregressive modeling techniques assume that the signal is stationary over the period of observation. This assumption is not correct in presence of non-synchronous interference, and is also inexact for distorted MSK signals (distorted by the premodulation and predetection filters). Moreover, the frequency separation between the user of interest and the interferers may be lower than the resolution of the parametric frequency estimator, which limits the performance of the MB receiver.

6.2 Suggestions for Future Work

The simulation results in presence of CCI were principally derived for the 8 EPB model-based technique and MSK signals. In this technique the receiver performs eight frequency estimations per bit (EPB) utilizing the Kumaresan and Tufts estimator after filtering, and tracks this instantaneous frequency with the Viterbi algorithm. The complexity of this technique has been discussed in Chapter 5 and is a major limitation to its implementation. Various techniques have been proposed in Chapter 4 to reduce the complexity of the MB demodulator (single estimation per bit; partial frequency response instead of the polynomial rooting). Further simulation is needed to evaluate the degradation of performance of the reduced complexity demodulator in presence of CCI. Also, a combined technique employing a coherent detector and low complexity MB detection could be implemented. The results of these diverse methods with CCI may be derived for MSK and GMSK signals.

The combined scheme proposed in Chapter 5 employs the model-based and the coherent detectors and jointly tracks the soft outputs of these two demodulation schemes. The performance improvement obtained by demodulation diversity is caused by the dissimilarity of the two techniques and their different behaviors in presence of CCI (low probability of common errors). Although a combined scheme employing the coherent technique and a conventional non-coherent technique, like the limiter-discriminator, may not provide as much improvement, it has been shown in [Las1997a] that this technique could still outperform the coherent detector. In [Las1997a] however, the use of sequence estimation with demodulation diversity combining has not been considered; a combined scheme employing the conventional coherent and non-coherent detectors and sequence estimation would have reasonable complexity and may achieve good performance.

There does not exist a perfect solution to the problem of co-channel interference rejection for MSK signals. The complexity of the optimum joint detection is prohibitive but sub-optimum techniques are unable to properly separate nearly equal-power users. It may also be questioned whether the complexity of the non-coherent MB technique is preferable to the phase synchronization process required for the coherent schemes. Finally, new demodulators for GMSK have recently been created based on Laurent decomposition. The representation of GMSK signal as a sum of PAM signal is promising as it permits the implementation of conventional multiuser detection techniques with acceptable complexity.

Bibliography

[Ada1988a] F. Adachi, K. Ohno, "Performance Analysis of GMSK Frequency Detection with Decision Feedback Equalization in Digital Land Mobile Radio", *Proceedings of the IEEE*, vol. 135, no. 3, pp. 199-207, June 1988

[Ada1988b] F. Adachi, K. Ohno, "Experiments on Postdetection Diversity for narrowband Digital FM Mobile Radio", *Electronics Letters*, vol. 24, no. 24, pp. 1491-1493, November 1988

[Ada1990] F. Adachi , K. Ohno, "Performance Evaluation of Various Decision Schemes for Frequency Demodulation of Narrow-Band Digital FM Signals in Land Mobile Radio", *IEEE Transactions on Vehicular Technology*, vol. 39, no. 2, pp. 109-116, May 1990

[And1986] J. B. Anderson, T. Aulin, C. E. Sundberg, *Digital Phase Modulation*, Plenum Press, New York, NY, 1986

[Ars2000] H. Arslan, K. Molnar, "Iterative Cochannel Interference Cancellation in Narrowband Mobile Radio Systems", *IEEE Emerging Technology Symposium on Broadband, Wireless Internet Access*, April 2000

[Ars2001] H. Arslan, K. Molnar, "Cochannel Interference Suppression with Successive Cancellation in Narrow-Band Systems", *IEEE Communications Letters*, vol. 5, no. 2, pp. 37-39, February 2001

[Bay2000] S. Bayram, *Overloaded Array Processing: System Analysis, Signal Extraction Techniques, and Time-Delay Estimation*, Master Thesis, Virginia Polytechnic Institute and State University, December 2000

[Ben1999] S. Benedetto, E. Biglieri, *Principles of Digital Transmission With Wireless Applications*, Kluwer Academic / Plenum Publishers, New York, NY, 1999

[Boa1992a] B. Boashash, "Estimating and Interpreting the Instantaneous Frequency of a Signal - Part 1: Algorithms and Applications", *Proceedings of the IEEE*, vol. 80, no. 4, pp. 520-538, April 1992

[Boa1992b] B. Boashash, "Estimating and Interpreting the Instantaneous Frequency of a Signal - Part 2: Algorithms and Applications", *Proceedings of the IEEE*, vol. 80, no. 4, pp. 540-568, April 1992

[Chi1996] M. Chiani, "Performance of BPSK and GMSK with Multiple Cochannel Interferers", *7th IEEE International Symposium on Personal, Indoor and Mobile Radio Communications*, pp. 833-837, October 1996

[Cho1999] J. Chow, N.C. Beaulieu, "Analysis of Cochannel Interference in Angle Modulation Systems", *IEEE Pacific Rim Conference on Communications, Computers and Signal Processing*, pp. 123-127, August 1999

[Chu1984] K. S. Chung, "Generalized Tamed Frequency Modulation and its Application for Mobile Radio Communications", *IEEE Journal on Selected Areas in Communications*, vol. SAC-2, pp. 487-497, July 1984

[Clar1993] P. M. Clarkson, *Optimal and Adaptive Signal Processing*, CRC Press, Boca Raton, Fl, 1993

[Cou2001] L. W. Couch, *Digital and Analog Communication Systems*, 6th Edition, Prentice Hall, Upper Saddle River, NJ, 2001

[Gol1989] G. H. Golub, C. F. Van Loan, *Matrix Computations Second Edition*, The Johns Hopkins University Press, Baltimore, Ma, 1989

[Ham2000] J. Hamkins, "An Analytic Technique to Separate Cochannel FM Signals", *IEEE Transactions on Communications*, vol. 48, no. 4, pp. 543-546, April 2000

[Hay1996] S. Haykin, *Adaptive Filter Theory Third Edition*, Prentice Hall, Upper Saddle River, NJ, 1996

[Hir1984] M. Hirono, T. Miki, K. Murota, " Multilevel Decision Method for Band-Limited Digital FM with Limiter-Discriminator Detection", *IEEE Journal on Selected Areas in Communications*, vol. SAC-2, pp. 498-506, July 1984

[Iwa1995] Y. Iwanami, "Performance of Sequence Estimation Scheme of Narrowband Digital FM Signals with Limiter-Discriminator Detection", *IEEE Journal on Selected Areas in Communications*, vol. 13, no. 2, pp. 310-315, February 1995

[Jen1991] P. M. R. Jensen, *Singular Value Decomposition and its Application to Autoregressive Parametric Spectral Estimation*, Technical Report R91-33, Department of Communication Technology, Institute of Electronic Systems, Aalborg University, Denmark, August 1991

[Kay1988] S. M. Kay, *Modern Spectral Estimation Theory & Application*, Prentice Hall, Upper Saddle River, NJ, 1988

[Kay1993] S. M. Kay, *Fundamentals of Statistical Signal Processing Estimation Theory*, Prentice Hall, Upper Saddle River, NJ, 1993

[Kum1982a] R. Kumaresan, D. W. Tufts, "Estimating the Parameters of Exponentially Damped Sinusoids and Pole-Zero Modeling in Noise" *IEEE Transactions on*

Acoustics, Speech and Signal Processing, vol. ASSP-30, no. 6, pp. 833-840, December 1982

[Kum1982b] R. Kumaresan, D. W. Tufts, "Estimation of Frequencies of Multiple Sinusoids: Making Linear Prediction Perform Like Maximum Likelihood", *Proceedings of the IEEE*, vol. 79, no. 9, September 1982

[Las1997a] J. D. Laster, *Robust GMSK Demodulation Using Demodulator Diversity and BER Estimation*, PhD Dissertation, Virginia Polytechnic Institute and State University, Blacksburg, Va, March 1997

[Las1997b] J. D. Laster, J. H. Reed, "Interference Rejection in Digital Wireless Communications", *IEEE Signal Processing Magazine*, vol. 14, no. 3, pp. 37-62, May 1997

[Lau1986] P. A. Laurent, "Exact and Approximate Construction of Digital Phase Modulations by Superposition of Amplitude Modulated Pulses (AMP)", *IEEE Transactions on Communications*, vol. 34, no. 2, pp. 150-160, February 1986

[Lee1988] S.U. Lee, Y. M. Chung, J. M. Kim, "On the Bit Error Probabilities of GMSK in the Rayleigh Fading Channels", *IEEE 38th Vehicular Technology Conference*, pp. 249-254, June 1988

[Lop1991] L. P. Lopes "Coherent and Limiter-Discriminator Detection of GMSK in Interference Limited Conditions", *Electronic Letters*, vol. 27, no. 25, pp. 2313-2315, December 1991

[Mur1981] K. Murota, K. Hirade, "GMSK Modulation for Digital Mobile Radio Telephony", *IEEE Transactions on Communications*, vol. 29, no. 7, pp. 1044-1050, July 1981

[Mur1995] P. A. Murphy, G. E. Ford, "Cochannel Demodulation for Continuous Phase Modulated Signals", *Proceedings of the 28th Asilomar Conference on Signals, Systems, and Computers*, 1995

[Mur1996] P.A. Murphy and G.E. Ford, "Cochannel Receivers for CPM Signals Based Upon the Laurent Representation," *Proceedings Virginia Tech's 6th Symposium on Wireless Personal Communications*, Blacksburg, VA, June 1996

[Pro2001] J. G. Proakis, *Digital Communications Fourth Edition*, McGraw-Hill, New York, NY, 2001

[Ran1995] P. A. Ranta, A. Hottinen, Z. C. Honkasalo, "Co-Channel Interference Canceling Receiver for TDMA Mobile Systems", *IEEE International Conference on Communications*, vol. 1, 1995

[Rap1996] T. S. Rappaport, *Wireless Communications*, Prentice Hall PTR, Upper Saddle River, NJ, 1996

[Rim1988] B. E. Rimoldi, "A Decomposition Approach to CPM", *IEEE Transactions on Information Theory*, vol. 34, no. 2, pp. 260-270, March 1988

[Sim1983] M. K. Simon, C. C. Wang, "Differential Versus Limiter Discriminator Detection of Narrowband FM", *IEEE Transactions on Communications*, vol. 31, no. 11, November 1983

[Sim1984] M. K. Simon, C. C. Wang, "Two-Bit Differential Detection of MSK", *GLOBECOM '84 Conference Record*, pp. 2231-2236, December 1984

[Skl1988] B. Sklar, *Digital Communications Fundamentals and Applications*, Prentice Hall, Upper Saddle River, NJ, 1988

[Sto1997] P. Stoica, R. L. Moses, *Introduction to Spectral Analysis*, Prentice Hall, Upper Saddle River, NJ, 1997

[Suz1981] H. Suzuki, "Optimum Gaussian Filter for Differential Detection of MSK", *IEEE Transactions on Communications*, vol. 29, no. 6, pp. 916-918, June 1981

[The1992] C. W. Therrien, *Discrete Random Signals and Statistical Signal Processing*, Prentice Hall, Upper Saddle River, NJ, 1992

[Tun1994] C. C. Tung, J. N. Livingston, "Viterbi Detector for Narrow-Band Digital FM with Limiter-Discriminator Detection", *GLOBECOM '94 Conference Record*, pp. 201-205, 1994

[Vas2000] S. V. Vaseghi, *Advanced Digital Signal Processing and Noise Reduction, Second Edition*, John Wiley & Sons, New York, NY, 2000

[Ver1998] S. Verdu, *Multiuser Detection*, Cambridge University Press, Cambridge, UK, 1998

[Wel1996] M. L. Welborn, *Co-Channel Interference Rejection Using a Model-based Demodulator*, Master Thesis, Virginia Polytechnic Institute and State University, Blacksburg, Va, January 1996

[Yao1996] S. K. Yao, J. H. Reed, J. D. Laster, "GMSK Differential Detectors with Decision Feedback in Multipath and CCI Channels", *GLOBECOM '96 Conference Record*, 1996, vol. 3, pp.1830 -1834, 1996

[Yon1988] A. Yongacoglu, D. Makrakis, K. Feher, "Differential Detection of GMSK Using Decision Feedback", *IEEE Transactions on Communications*, vol. 36, no. 6, pp. 644-649, June 1988

Vita

Pierre Barthélemy was born on November 6, 1978, in Evry, France. He attended Lycée Chaptal, Paris, France and transferred to the Ecole Supérieure d'Electricité (SUPELEC), Metz, France in 1998. He received his Engineering Degree from SUPELEC in July 2002. From August 2000 to May 2002, he attended Virginia Polytechnic Institute and State University Graduate School. Pierre joined the Mobile and Portable Radio Research Group (MPRG) in January 2001. He received his Master of Science Degree from Virginia Tech in May 2002 under Dr Brian D. Woerner. His research interests include digital signal processing, multiuser detection and modulation.